PHYSICAL MODEL STUDIES OF METACHRONAL SWIMMING

By

HONG KUAN LAI

Bachelor of Science in Mechanical Engineering

Oklahoma State University

Stillwater, Oklahoma

2014

Submitted to the Faculty of the
Graduate College of the
Oklahoma State University
in partial fulfillment of
the requirements for
the Degree of
MASTER OF SCIENCE
December, 2016

PHYSICAL MODEL STUDIES OF METACHRONAL SWIMMING

Thesis Approved:

Dr. Arvind Santhanakrishnan

Thesis Adviser

Dr. Jamey Jacob

Dr. Ronald Delahoussaye

ACKNOWLEDGEMENT

I take this opportunity to express my sincere and deepest appreciation to my committee chair, adviser, mentor and more importantly a great friend Dr. Arvind Santhanakrishnan. I thank him for introducing me to the wonders of research. I thank him for his guidance, encouragement and support right from the beginning of this work. I thank him for his supervision and constant help, without which this thesis would not have been possible.

I would like to thank my committee members Dr. Jamey Jacob and Dr. Ronald Delahoussaye. They have provided, with kindness, their insight, suggestions and support, which are precious to me.

I place on record, my sincere thank you to Dr. Daniel Fisher, Head of the School of Mechanical and Aerospace Engineering, for the continuous encouragement.

I am also grateful to Aaron Alexander, Assistant Professor of Mechanical Engineering Technology. I am extremely thankful and indebted to him for sharing his expertise, and valuable guidance all through my master's education.

Special thanks are due to all the past and present members of Applied Fluid Mechanics Laboratory (AFML) at Oklahoma state university. Especially, Audrey Pope, Indah Merkel, Alice Montague, Blake Baber, and Milad Samaee for their support and friendship.

Name: HONG KUAN LAI

Date of Degree: DECEMBER, 2016

Title of Study: PHYSICAL MODEL STUDIES OF METACHRONAL SWIMMING

Major Field: MECHANICAL ENGINEERING

Abstract: Aquatic crustaceans such as copepods, krill and shrimp spend most of their life cycle swimming. These organisms have been studied for their ecological importance, as they form a crucial link between smaller phytoplankton and larger, commercially important fishes. Crustaceans employ a unique drag-based strategy for swimming in which 4-5 closely spaced pairs of limbs are periodically oscillated in the tail to head direction. Each of their swimming limbs (pleopods) are phase-shifted in time relative to the neighboring limb, resulting in a metachronal wave traveling in the same direction as the animal. We developed a dynamically scaled robotic model of metachronal swimming to investigate: 1) Reynolds number (Re) scalability of the mechanism, and 2) the importance of inter-pleopod spacing and stroke amplitude (SA) on swimming hydrodynamics. The tethered robotic model consisted of acrylic linkages and plastic bevel gears mounted on a base plate. Physical models of pleopods were constructed using acrylic plates with hinges, to mimic the asymmetric pleopod deformation observed in power and recovery strokes of swimming. The entire assembly was mounted on top of a glass aquarium filled with water-glycerin fluid mixtures of varying viscosities for dynamic scaling. 2D particle image velocimetry (PIV) measurements across Re ranging from 10 to 1000 showed that propulsive flows change from horizontally oriented (thrust-generating) at low Re to angled vertical jets (lift-generating) at larger Re. Adult crustaceans typically need to contend with negative buoyancy, and thus this finding suggests that the propulsive jets can aid in weight support as well as thrust generation. The inter-pleopod gap to pleopod length ratio (G/L) in metachronal swimmers has been observed to be within a narrow range of 0.2-0.65. We used 2D PIV to examine the effect of varying G/L on the propulsive flows. Our results showed that synergistic hydrodynamic interactions occur between adjacent pleopods in the form of alternating suction and expulsion jets. For a given design G/L and Re, increasing SA resulted in augmenting thrust-generating flow. For the maximum SA and largest Re investigated, the lowest G/L ratio case showed lift-generating flow, suggesting that synergistic interactions can modulate the propulsive flow direction in metachrony.

TABLE OF CONTENTS

Chapter Page

Chapter Page

LIST OF TABLES

Table Page

LIST OF FIGURES

Figure Page

Figure Page

Figure Page

Figure Page

Figure Page

`

CHAPTER I

INTRODUCTION

1.1 Motivation

There are over 3,000 satellites orbiting the earth today for covering 196.9 million square miles of area; yet only one autonomous under water vehicle (AUV) was used most of the time in search missions for ship wreckage on the deep ocean floor. Due to cost of operations that limit the number of deployments, AUVs today take a substantial amount of time to cover large volumes. AUVs are typically big in size, which compromises maneuverability, but the most significant disadvantage of most commercial AUV designs is the use of a single propulsion element. Single propulsion element creates high reliability issue, as the entire mission will be comprised if the propulsion element fails. The other challenge for single propeller-based AUVs is the limited range of operation across different Reynolds number (Re) conditions, essentially achieved by modulating the rotational speed of the propeller. In order to improve the effectiveness of AUVs, new propulsion systems that are more reliable and operational in various conditions have to be established.

1.2 Bio-inspired AUV Design

A good way to redesign a propulsion system that operates in a vast range of water conditions efficiently is to look at locomotion strategies used by aquatic organisms. Aquatic animals such as fishes can use their back fins (also known as caudal fins) to move their body forward by flexing their body, with the help of muscle contraction and relaxation from side to side. This type of aquatic locomotion can be categorized as a lift-based locomotion, where the appendage (fin) oscillation is perpendicular to the direction of flow [Gibb et al. (1999)] [Yu et al. (2011)] [Hu et al. (2006)]. The other type of locomotion used by animals such as jellyfish and squid involves creating pulsating jets for propulsion [Nawroth et al. (2012)] [McHenry et al. (2003)] [Shorten et al. (2005)]. The downside to both of these locomotion systems in the context of bio-inspired AUV design is reliance on a single propulsion element, such as fish that use only one tail fin and jellyfish that use a single bell. The next challenge in using fish and jellyfish locomotion-based AUV design is the continuous structural deformations that occurs across most of the propulsion element (fin motion and bell pulsation). Mimicking this in an engineering device requires sophisticated flexible materials to be integrated into the design, which complicates the design process and increase cost of production. Therefore, an aquatic locomotion system with multiple propulsion elements, which also does not require a continuous change in material flexibility, are preferable for future low-cost AUV design.

1.3 Metachronal Paddling

Crustacean aquatic animals for example crayfish, krill, and shrimp use a tail to head metachronal wave motion to propel forward. These organisms have not been previously considered for bio-inspired AUV design. The propulsion mechanism for crustacean animals typically comes with 4 to 5 pairs of pleopods also known as swimmerets; this propulsion system is able to counter the issue of a single propeller design due to its ability to operate all pairs of limb independently of

each other. However, when working together, they always maintain in an out-of-phase-pace which means that each pair of limb will start a cycle in a delayed phase, compared to its neighboring paddle [Knight-jones et al. (1959)]. Even though a limb structure of crustacean aquatic animals consist of two major parts (prodopodite and endopodite) that expand to achieve maximum surface area during power stroke PS and bend to reduce drag during recovery stroke RS with the help of a hinged joint, these two major parts of limb structure do not require evolving surface change or flexing which introduces an easier design concept model of future AUV design. Besides that, another advantage of such a propulsion system was the range of Reynolds number Re that is able to operate from youth to adult size body. The scalability of metachronal paddling model for different sizes ranging from youth to adult will provide a good understanding of flow patterns generated to overcome different morphology and weight. In order to understand the fundamentals of how metachronal paddling works and how this model contributes to the flow around its swimming body, the best practice is to simplify crustaceans' swimming model in order to itemize the question and investigate them individually.

1.4 Specific Aims

25 % phase difference were tested to be the most efficient metachronal paddling model for a four-limb design from the perspective of computational neuro-circuit mechanism design done by [Zhang et al. (2014)]. The downside of most kinds of computational design was the difficulty of modeling power stroke and recovery stroke of limb structure which involved computing continuous surface area changes by stretching and bending limb Endopodite relative to the flow generated around the paddle. Due to this difficulty, most types of computational design set up experiment with permeable and non-permeable paddles. The goal of this study is to model limb structures that are similar to what is observed in real life crustacean swimming by building a physical model with a pleopod-like paddle structures submerged into a test volume to truly test the hydrodynamics of metachronal paddling. The physical model done for this study only focuses

on four pleopod structures by designing pleopod-like paddles made up of acrylic material joined halfway by a hinge. Implementing a hinged design will ensure that all four paddles perform power stroke and recovery stroke oscillation with prodopodite section propels fluid in the test volume and endopodite section influences freely by the flow around it.

The different range of size and weight of crustacean animal sharing the similar locomotion system suggests the idea of downward generating flow during metachronal paddling motion in order to keep negatively buoyant body afloat. An experimental study from [Murphy et al. (2013)] [Catton et al. (2011)] looked into real life krill and found out that there is present of angled downward generating flow in order to hover in a water column confinement. This will answer the question of future AUV design that can come with different sizes and still operate smoothly and maintain depth altitude. Two major aims are being introduced in this study to tackle the problem of scalability of metachronal paddling in relation with different body sizes.

The first aim of this study is to look at body size variation in terms of fluid Reynolds number experienced by each limb on physical model in the test volume. For a small body size animal, the Reynolds number of fluid surrounding its limb should be a lot lower compare to a larger body size, hence a lower Re number produces a higher viscosity number value. 3 Reynolds number (Re50, 250, 800) in the order of 10 (baby size), and 100 (adult size) was chosen based on the Re range experienced by tip of pleopod in typical crustacean animals. By maintaining the oscillation motion of the physical limb and other constant variables, for example limb length and gap, Re number, will allow the understanding of scalability through pleopod to fluid hydrodynamics interaction.

The second aim of this study also tackle the understanding of scalability of metachronal paddling motion, but from a different perspective. Aim 2 study scalability by not looking at how physical pleopod structures interact with different fluid condition, nonetheless this study look at how

different pleopod gap to length ratio interact with constant fluid Re number. Typical crustacean aquatic animals stayed between a pleopod gap to length ratio of (0.2-0.65) [Murphy et al. (2011)]. This study will explore the scalability of metachronal paddling in terms of the ratio between pleopod to the length of each pleopod to simulate how different limb geometry are able to interact with the fluid around them in order to swim or stay afloat.

This experiment study proposed will be a valuable key to solve the problem of current AUVs design. The future vision of an autonomous underwater vehicle should be able to alter its metachronal paddling behavior by changing variables like, limb oscillation, limb gap, and limb phase difference to adapt in any water conditions, therefore starting from the basic of understanding metachronal paddling motion, will help setup a platform for future AUV design.

CHAPTER II

LITERATURE REVIEW

2.1 Motivation

Autonomous underwater vehicle (AUV) is use most of the time in search and exploration missions on the vast deep ocean floor. Underwater vehicles for search missions normally range between 1.8 m to 13 m and they operate in depths ranging from 2 km to 1500 km [Eriksen et al. (2001)][Prestero, Timothy (2001)][Yoerger et al. (2007)][McGann et al. (2009)]. Due to the high cost of AUVs, search missions normally only involve one vehicle, which spends too much time to achieve adequate coverage progress. For a large sized AUV, maneuverability of vehicle that requires operational functions in tough environments is an issue. Beside issues with maneuverability, the most significant disadvantage of AUV design today is the single propeller propulsion system. Single propulsion system for such an important mission generates high reliability risk and the mission will more likely fail if the whole system depends only on one propeller. The other challenge for single propeller AUVs is the limited operational Reynolds number (Re) ranges which was mainly constrained by the propeller's rotational speed [Yoerger et al. (1990)][Alvavez et al (2009)]. The limitation of single propeller propulsion system stresses the urge for further development and improvement for future AUV design. In order to improve the effectiveness of AUVs, new propulsion systems that are more reliable and operational in various conditions have to be established.

A good way to redesign a propulsion system that can conquer vast ranges of Re condition efficiently is to look at example of bio-inspired designs from nature. Aquatic animals that have adapted certain swimming styles might be a helpful clue to solve the current problem in AUV design.

2.2 Underwater Bio-propulsion

The wide range of aquatic species with various swimming styles could be useful to solve problems faced by current AUVs. Swimming styles that are adapted naturally by certain species over the years suggest strong efficiency in fulfilling its task; and the ideal locomotion technique needed should address issues on high reliability of single propulsion system and increase the operational Re range.

2.2.1 Types of swimming

Aquatic animals with appendages for propulsion are typically categorized into lift-based and drag-based [JA Walker (2002)] [Fish, Frank E (1996)]. Lift-based propulsion is defined when a swimming mechanism moves to propel the body forward by moving in a direction perpendicular to the body's travel direction. Examples of lift-based propulsion are fish [Sfakiotakis et al. (1999)] and Sea butterfly [Murphy et al. (2016)]. Drag-based propulsion on the other hand is defined with a swimming mechanism moving parallel to body direction similar to examples like Mayfly [Larson et al. (2014)], and krill [Murphy et al. (2011)].

2.2.2 Lift-based propulsion

A large number of studies on bio-propulsion have examined lift-based locomotion, [Gibb et al. (1999)] [Yu et al. (2011)] [Hu et al. (2006)] such as the undulation of tail fins from fishes as well as [Nawroth et al. (2012)] [McHenry et al. (2003)] [Shorten et al. (2005)] bell pulsation of prolate from jellyfish. The downside to both of these locomotion systems is that, fish that use only one

tail fin and jellyfish with only one pulsing bell, does not address the problem of the single propeller element in modern AUV design. The next disadvantage of fish and jellyfish designs is the continuous change of body and bell movement in order to swim forward, which requires a whole new level of flexible material-integrated design that actually complicates the design process and increases the cost of production.

2.3 Drag-based propulsion of crustacean swimming

Crustacean aquatic animals for example krill, crayfish, and shrimp share a same unique way of swimming which involves multiple pleopodal structure working together to push flow toward the tail. Each pleopod coordinates with neighboring pleopods efficiently in order to maximize generation of thrust; but at the same time each pleopod is able to operate individually on its own. Many papers [Alben et al. (2010)][Zhang et al. (2014)][Catton et al. (2011)] have looked into crustacean swimming methods and indicate that crustacean swimming style can be implemented in future AUV design.

2.3.1 Anatomy of pleopods

Crustaceans typically have four to five pairs of swimming limbs (pleopods), as shown in figure 1. Each pleopod can be divided into two major parts, an upper portion (prodopodite) and lower portion (endopodite). The prodopodite structure is attach to the abdomen portion of the body and this structure is considered rigid. Endopodite structures are more flexible and are not controlled by the abdomen muscles, rather the endopodite is free to move with the influence of flow around it.

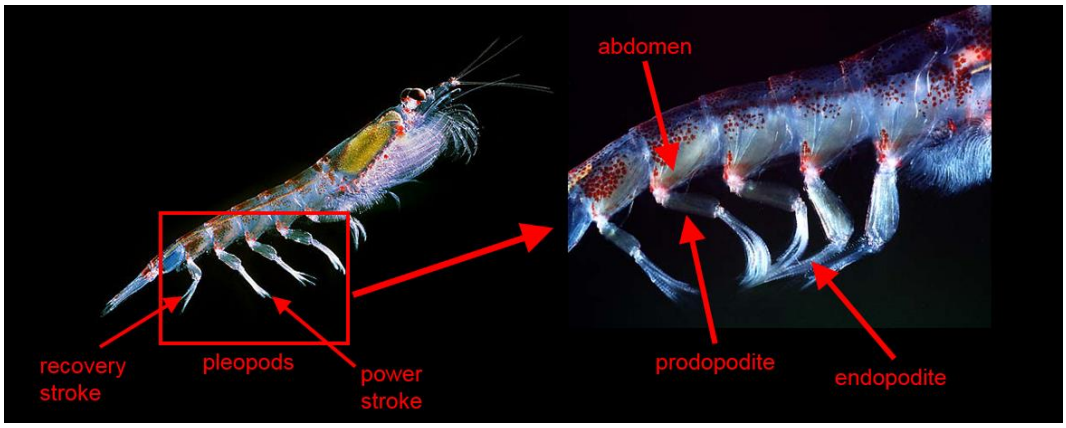

Figure 1 Anatomy of pleopod structures in krill. Picture were taken from Kristin Urquiza, Lifeline Antarctica 2016 Picture from Mission Blue Slyvia Earle Alliance & Uwe Kils 2005, "The pleopods" wikisource

2.3.2 Physiology of plepods

During swimming, each pleopod will oscillate back and forth with the origin located at the joint between abdomen and prodopodite. The oscillation of pleopod can be categorize into two stages, power stroke (PS) and recovery stroke (RS). PS starts with the direction where the pleopod moves from head to tail, and the RS process starts when the pleopods move from tail to head direction. Prodopodites and endopodites both expand to achieve maximum surface area during PS for maximum drag thrust and bend to reduce drag during RS thus generating differential drag. These two major parts of pleopod structure do not require evolving surface change or flexing which introduce an easier design concept to implement on AUV design.

2.4 Metachronal propulsion

Crustaceans swim with multiple pairs of pleopods together forming a metachronal wave motion. Metachronal swimming is defined when pleopod structures are oscillated out-of-phase relative to each other, which means each pair of pleopods will start its cycle in a delayed phase compared to its neighboring pleopod. The delayed sequence or the metachronal wave can be seen having a tail to head motion [Knight-jones et al. (1959)]. Tail to head metachronal wave is defined when the

pleopod closest to the tail start its PS cycle before its neighboring pleopod, and ends with the pleopod closest to the head starting PS. The metachronal wave is continuous throughout the swimming process in most crustaceans. A complete 100% stroke cycle of an individual pleopod is when pleopod structures start and return to the same position in an oscillation cycle. Normally, the out-of-phase-pace delay for each individual pleopod also known as percentage phase difference, can be argued to the resulting total of 100% cycle divide by number of pairs of pleopods. Alben et al. (2010) looked into krill with five pairs of pleopods and the tracked kinematics of pleopod turned out to be close to 20% phase difference. For a four pair pleopod structure model, the ideal phase difference between each pleopod should be 25% [Zhang et al. (2014)].

CHAPTER III

REYNOLDS NUMBER SCALABILITY OF METACHRONAL PADDLING

3.1 Abstract

Crustacean aquatic animals for example krill, crayfish and shrimp ranging from youth to adult stage, spend most of their time swimming and staying afloat. The question on how metachronal paddling with a tail to head wave motion for a smaller body that is neutrally buoyant, sharing the same methods of locomotion compared to a negatively buoyant adult size, is yet to be investigated thoroughly. The objective of this study is to build a physical model that is submergible in water-glycerin solution to study the propulsion system which typically consists of 4 to 5 pairs of pleopods. In order to support the idea of vertical flow being created for larger size system in order to stay afloat, a four-bar mechanism was designed to provide consistent oscillation of pleopod-like structures made up of hinged acrylic plates to mimic real life power stroke and recovery stroke. The variation of size was set up with changing Reynolds number experienced by each pleopod, in order to look into the hydrodynamics of metachronal paddling. Particle Imaging Velocimetry PIV techniques when acquiring 3 vertical planes within test volume showed increasing of velocity vectors and vorticity contours at higher Re number as well as the present of higher vertical flow. When looking at the ratio of lift to thrust coefficient, the trend showed to increase as well as Re number increases.

3.2 Introduction

Crustaceans such as krill, crayfish, and shrimp exhibit a range of sizes from larval to adult stage and krill for example spend up to 73% of their total daily energy expenditure on swimming [Swadling et al. (2005)] [Kils (1981)]. Crustacean uses a unique swimming style known as metachronal paddling which defined when pleopod structures move in an out-of-phase tail to head sequence with a delay period between one pleopod to the other [Knight-jones et al. (1959)]. This type of paddling motion which involves swimming pleopods to paddle in the direction of body movement, suggests a drag-based propulsion system [JA Walker (2002)]. The variation of size in crustacean species and it's pleopod oscillation frequency leads to Re number ranging from 10 to 1000 [Zhang et al. (2014)]. The question on how changes in size from larval to adult stage, use the same locomotion technique during swimming has not been examined carefully. A large number of studies on bio-propulsion have examined lift-based locomotion, [Gibb et al. (1999)] [Yu et al. (2011)] [Hu et al. (2006)] such as the undulation of tail fins in fishes as well as [Nawroth et al. (2012)] [McHenry et al. (2003)] [Shorten et al. (2005)] bell pulsation of prolate in jellyfish. The uniqueness of crustaceans' drag-based swimming typically consist of 4 to 5 pairs of swimming pleopods, but in the case of larval stage for example brine shrimp [T.A William (1994)] or polychaete worms [Clark et al. (1970)], only start out with few pairs of limb and more limbs will be added with development of size . This brings up the question of scalability of metachronal swimming model and how it will perform within a large range of sizes.

Murphy et al. (2013) looked into Antarctic krill that weighs higher than the density of surrounding fluid and study how they overcome their negatively buoyant body with the help of analyzing the wake of flow during metachronal paddling motion. In the paper of [Catton et al. (2011)], downward jet was discussed to the advantage of groups of krill swimming together to improve hydrodynamics of coordinated swimming in krill schools. These papers explained metachronal paddling with the observation of downward jet, but inter-pleopod flows were not

investigated to examine potential for synergistic interaction between pleopods undergoing metachrony. Finally, the consistency and repeatability of in vivo experiments are hard to achieve, therefore alternative approach to study metachronal paddling motion using computational and physical module could be highly valuable.

In contrast to in vivo studies, mathematical modeling of numerical simulations have been used to investigate the performance of metachronal paddling. A version with four 2D paddles [Zhang et al. (2014)] and the other with two paddle legs [Alben et al. (2010)] were modeled to compare metachrony with synchronous paddling. The result in Zhang's study showed higher net volumetric flux pushed towards the tail in the case of metachronal paddling and Alben's study showed higher body velocities as well. The interaction between adjacent paddles was explained on the basis of the geometry, such that fluid was essentially scooped by each paddle and transferred backward towards the tail. However, contrast to in vivo studies there was no observation of downward jet from these computational model. One limitation of computational model was the difficulty to realistically simulate limb structural power stroke (PS) and recovery stroke (RS). Crustacean pleopods consist of two major parts, an upper part (prodopodite) and a lower part (endopodite). The pleopods stretch out during PS for maximizing drag surface area and bend during RS to minimize surface area thus generating differential drag. In the study from [Daisuke Takagi (2015)] looked into modelling two or more rigid paddles and have shown successful result for metachronal paddling in moving flow, but the effects of a two part pleopods and downward generating jet observed from in vivo studies was not discussed. The reason most computational model go with permeable and non-permeable or rigid paddle design is due to the difficulty of modeling a rigid prodopodite that oscillates in metachrony together with a free moving endopodite that bends with the surrounding fluid.

The idea of using an idealized kinematics of each pleopod motion similar to what was modeled in a computational study but testing the metachrony wave motion in a real world condition, provides a higher valuability in understanding of crustacean locomotion. In this study, we developed a physical model with four artificial pleopod-like structures that were electronically driven to mimic metachronal paddling. The physical model was placed in a tank containing water-glycerin mixture for dynamic scaling of Reynolds number. Re number of individual paddles varies from order of 10 to order of 100 to examine scalability with changing size. Our result shows the inter-paddle jets interaction as well as the generation of downward jet similar to in vivo studies, and increasing the Re number altered the direction of the overall flow from a more narrow vertical jet to a more wider angled downward jet towards the tail.

3.3 Methods

3.3.1 Physical Model

Four pleopod-like structures also known as paddle design in this study were closely based on crustaceans that moves in an idealized back and forth motion, with a 50% power stroke (PS) and 50% recovery stroke (RS) [Zhang et al. (2014)]. The PS moved in an opposite direction to the body's swimming direction which can also be explained with a head to tail motion, whereas in RS (tail to head motion) the paddle moved in the same direction as the swimming direction [Alben et al. (2010)]. The physical model for this study was setup throughout all experiments with PS starting from left to right which simulates the head on the left and tail on the right. The next challenge of modeling surface area changes during PS and RS motion were addressed with implementation of hinged paddle design. Paddles were designed to expend to the max during PS to maximize drag surface area and bend during RS for the effectiveness of net flow toward the back of the body [Murphy et al. (2013)]. Each paddle consisted of two pieces of 1.91 cm length acrylic plate joined together with a hinge for a total of 3.81 cm length during PS.

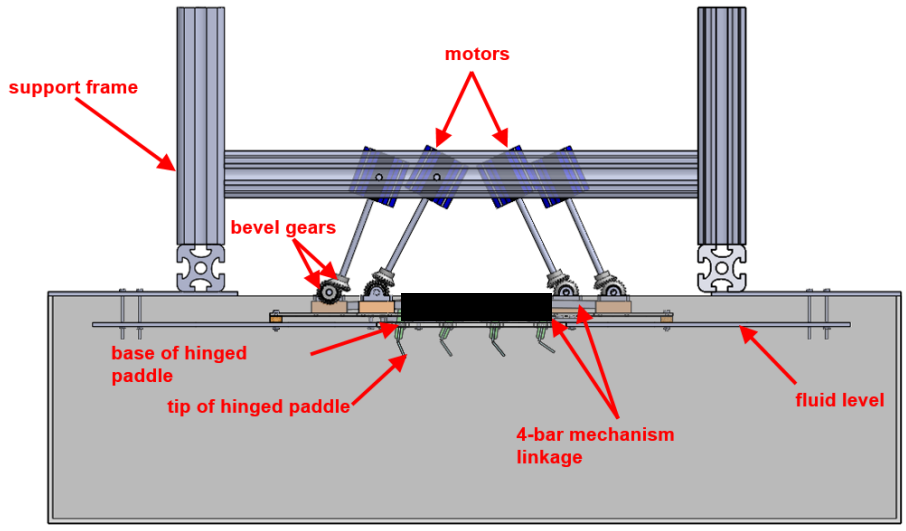

Figure 2 Schematic of experimental physical model which consist of 3 major parts. (i) 12-gallon test aquarium, (ii) Four sets of 4-bar mechanism, and (iii) Support frame for mounting four programmable motors.

In order to achieve a repeatable oscillating motion, a four-bar mechanism consisting of acrylic linkages were fabricated and mounted on a base plate shown in figure 2 such that the paddle rotate about an axis intersecting with fluid level. The two linkages were 1.53 cm and 7.62 cm in length. This combination allowed a total stroke amplitude of 90° with $\pm$45° motion referenced from center vertical axis. When four similar four-bar mechanisms were put together with 5.08 cm gap between each mechanism with all four paddles moving in an out-of-phase-pace, metachronal paddling motion was demonstrated. Four programmable motors (ST23-4E, National Instrument, Austin TX, USA) were used to drive shaft connected to four-bar mechanism. Support frame (80/20 inc, Columbia city, IN, USA) was used to allocate four programmable motors at its needed position. Physical model assembly was mounted in a 45-liter glass tank (90 cm x 21 cm x 24 cm) (Mr. Aqua Co. Ltd, California, USA).

3.3.2 Reynolds number calculation and calibration

Reynolds number Re was changed in experiments as a way to simulate variation of size by alternating only fluid viscosity. Water and glycerin mixtures were used to mimic different Re conditions experienced by the paddle. The Re formula used for calculation involved the amplitude (amp) of the angle of stroke experienced by the paddle tip at the maximum angular velocity which was $\pi/4$. The reported formula was $[Re = (L_{leg}) * (L_{leg} * 2 * \pi * amp/T)/v]$ (i) where paddle length (L_{leg}) as well as period of cycle (T) stayed constant on all experiment runs. Kinematic viscosity (v) was changed using multiple combination of water-glycerin solution.

$v\ (cm^2/s)$	*Re*	% error *Re*
7.56E-05	50	5.24
1.33E-05	250	7.34
4.39E-06	800	2.07

Table 1 Constant variables (i) The period of paddle oscillation was set to a constant of 2s, (ii) The paddle length was fixed at 3.81 cm, (iii) Hinged point was set to split the paddle in 50-50 ratio.

3.3.3 Kinematics

The main purpose of kinematics was to validate all four paddle's kinematics motion on physical model. Alben et al. (2010) looked into the kinematics of krill with 5 pleopods, the phase difference of the upper haft of pleopod maintained close to 20% phase difference between each pleopod to the other. In the other study done by [Murphy et al. (2011)] showed similar phase difference for upper-pleopod for a five pleopods E. superba. By referencing to [Zhang et al. (2014)] which worked on computational design on four 2D pleopod-like paddles, the paddle for physical model in this study was set with an idealized motion profile of 25% phase difference. The physical model used in this paper was designed to run with metachrony close to 25% phase difference, due to the resulting total of 100% stoke cycle dividing by the number of pleopods. In order to validate the motion on physical model, a custom Matlab code from [T.L Hedrick (2008)] was used for two- dimensional tracking of high-speed videos. Information outputted with pixel by pixel coordinates of each tracked points can be converted to length scale and degree with careful calibration while recording. In each video frame, 8 points were tracked with 2 points on each of the four paddles [(1) midpoint between upper paddle (Protopodite) and lower paddle (Endopodite), (2) tip of paddle]. By using tracked points, the kinematics of the paddle was tracked and plotted.

3.3.4 PIV

Two-dimensional time- resolved particle image velocimetry (2D TR PIV) was used to visualized inter-pleopods flow and flow of the wake during metachronal paddling cycle. A schematic of the PIV experiment setup is shown in figure 3. Glass hollow spheres (110P8, LAVISION GMBH, Goettingen,Germany) were used as seeding particles inside the test volume. Three vertical PIV planes ((P_{V1}) center plane of tank, (P_{V2}) 1.27 cm away from center plane Particle Image & (P_{V3}) 3.81 cm away from center plane) were setup. All three vertical PIV planes was illuminated using

a double pulse laser, single cavity Nd:YAG laser (Photonics Industry Inc., NY, USA) that provided a 0.5mm beam of 527nm in wavelength. A cylindrical lens (10mm focal length) was used to make planer laser sheet from laser beam. A sCMOS0 camera (2600 x 2200 pixels, LAVISION Inc., Ypsilanti, Michigan, USA) was positioned in front of the physical model and focused on the seeding particles using a 60mm constant focal length lens (Nikon Micro Nikkor, Nikon Corporation, Tokyo, Japan). The aperture of camera lens was set on 2.8 for all experiment. A signal outputted from all 4 motors at the beginning of each cycle is linked with the programmable time unit (PTU) as a starting trigger in order to acquire data at the same starting point. The PIV particle size was in the range of 1.5-3 pixels. For each experiment, 20 raw PIV images per cycle were recorded with a camera frame rate of 10 frames per second. 50 cycles per experiment were taken with 5 sets of 10 cycles each due to the limitation of storing memory power. Particle displacements in the test volume ranged between 4-7 pixels. The physical model was allowed to run continuously for over 100 pleopod stroke cycle before acquisition of PIV data. Raw PIV images were processed using Davis 8.3.0 software (LaVision GmbH, Gottingen, Germany). The processed velocity vectors fields were averaged for 50 cycles. Multi-pass cross-correlation was performed on the PIV data with initial window size of 64x64 pixels (2 passes) to final window size of 32x32 (2 passes) with 50% overlap.

Post-processing was performed by rejecting velocity vectors with peak ratio less than 1.2 and interpolation was used to replace empty vectors. Two dimensional velocity components (u in x direction, and v- in y direction) of flow in the test volume were obtained after PIV averaging.

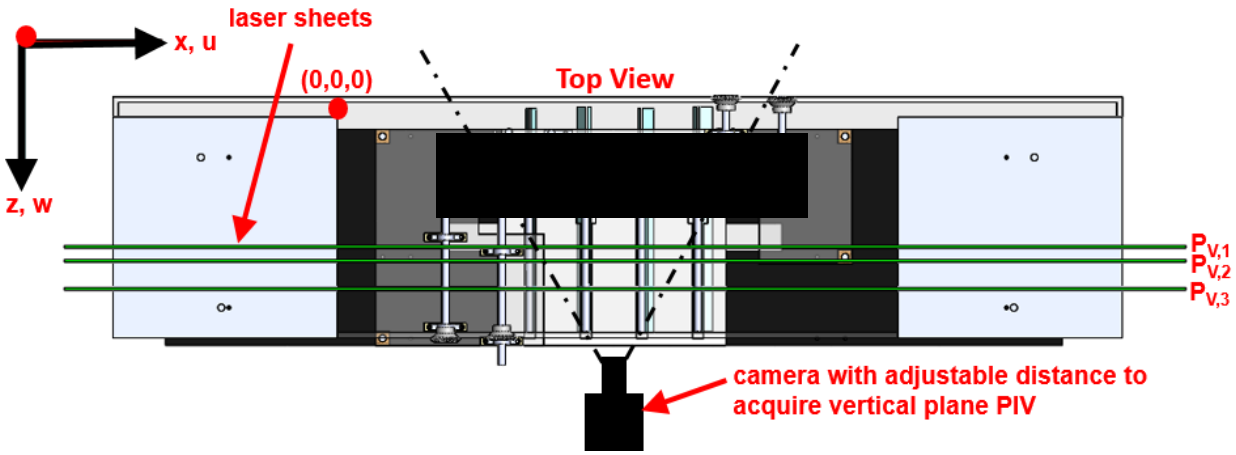

Figure 3 shows front and top view on where laser sheets plane are located during PIV acquisition. PV,1, 2 & 3 represents vertical laser planes parallel to the front of the tank with location at center of the tank, 1.27cm away from center and 3.81cm away from center.

3.3.5 Definition of calculated quantities

3.3.5.1 Pleopods angle kinematics

Eight points were tracked on physical model in order to acquire coordinated change of each hinged paddle throughout a stroke cycle. The schematic of tracked point was showed in figure 4

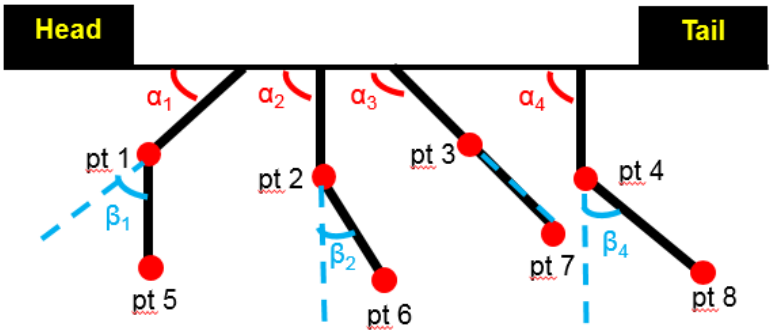

Figure 4 Kinematics references for tracking changes in angles throughout stroke cycle

The angles α and β can be obtained for a stroke cycle by using angle formula as defined:

$$\alpha_n = \tan^{-1}\left[\frac{(y(paddle_n\ root) - y(ptn))}{(x(paddle_n\ root) - x(ptn))}\right] \ for\ x(paddle_n\ root) > x(ptn) - - - (ii)$$

$$\alpha_n = 180 - \tan^{-1}\left[\frac{(y(paddle_n\ root) - y(ptn))}{(x(paddle_n\ root) - x(ptn))}\right]\ for\ x\ < x(ptn) - - - (iii)$$

$$\beta_n = 90 - \tan^{-1}\left[\frac{(y(ptn) - y(pt(n+4)}{(x(ptn) - x(pt(n+4)}\right] - - - (iv)$$

3.3.5.2 Vorticity

Out of plane z-vorticity, ω_Z was calculated using:

$$\omega_Z = \frac{\partial v}{\partial x} - \frac{\partial u}{\partial y} - - - (v)$$

3.3.5.3 Momentum Flux F_x &F_y

The momentum Flux calculation was set up as shown in figure 5. The left and right most boundaries were set at one paddle length scale away from the first and fourth paddle starting from left. The bottom boundary was set close to the bottom wall of the tank to capture the full effect of vertical flux.

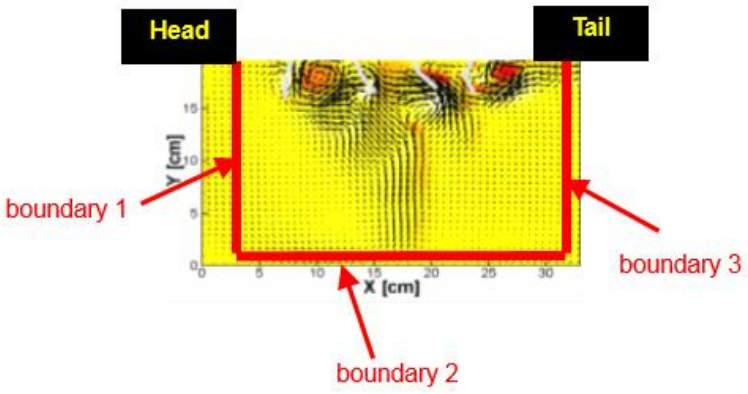

Figure 5 Momentum flux calculation with boundaries was set up. Left and right boundaries were one length scale away from 1st and 4th paddle. The bottom boundary was set to be closest to the bottom of the tank.

With the boundaries set up, horizontal and vertical momentum flux can be calculated with the as shown below:

$$\frac{\partial}{\partial t}\int_{cv}\rho u\,dV + \int_{cs}\rho u(\vec{u}\cdot\hat{n})dy = \sum F_x \quad (vi)$$

(0 under time averaging)

$$\sum F_x = \left[-\rho\sum_1 u^2dy\right] - \left[\rho\sum_2 uvdx\right] + \left[\rho\sum_3 u^2dy\right] \quad (vii)$$

$$\frac{\partial}{\partial t}\int_{cv}\rho v\,dV + \int_{cs}\rho v(\vec{u}\cdot\hat{n})dy = \sum F_y \quad (viii)$$

(0 under time averaging)

$$\sum F_y = \left[-\rho\sum_1 uvdy\right] - \left[\rho\sum_2 v^2dy\right] + \left[\rho\sum_3 uvdy\right] \quad (ix)$$

3.3.5.4 Thrust Coefficient C_t & Lift Coefficient C_l

$$V = \frac{2\pi L(amp)f}{2} \quad (x)$$

$$C_t = \frac{\sum F_x}{\frac{1}{2}\rho V^2 L} \quad (xi)$$

$$C_l = \frac{\sum F_y}{\frac{1}{2}\rho V^2 L} \quad (xii)$$

3.4 Results

3.4.1 Kinematics of paddles on physical model.

Each paddle on physical model were recorded for 10 stroke cycles and were tracked to obtain kinematics using the equations from section 3.3.5.1. Eight points were tracked in each video with two points on each paddle [(i) hinged joint between upper paddle and lower paddle, (ii) tip of paddle] shown in figure 4. The result of angle α and β were plotted as shown in figure 6.

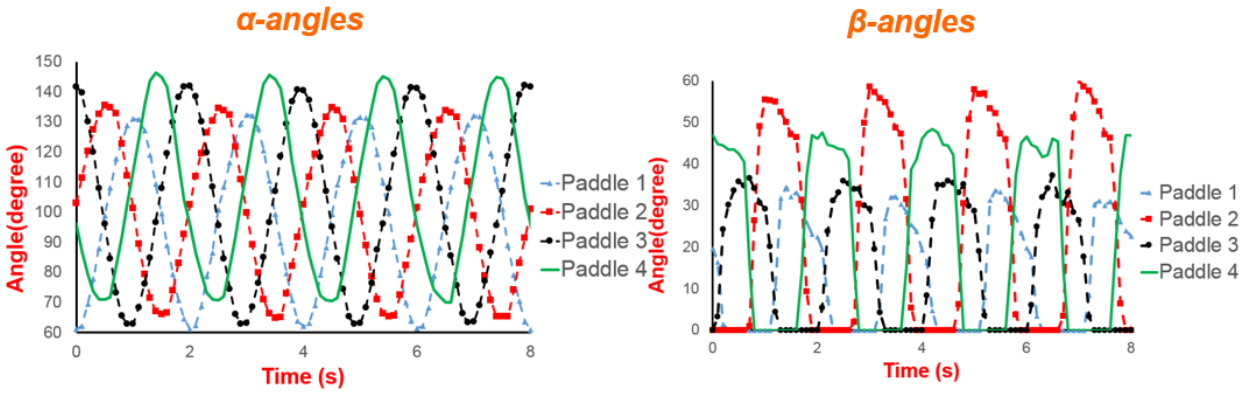

Figure 6 Kinematics from 4 stroke cycle were shown. Each α and β angle (paddle 1 closest to the head, paddle 4 closest to the tail) were plotted versus time. The kinematics of α angle for each paddle showed to be repeatable and close to 25% phase difference. B angle behaves in a noisier pattern and the kinematics will be different at each Re.

The kinematics plot in figure 6 for angle α showed to be repeatable and close to 25% phase difference between one paddle to other. The degree range for each paddle were slightly varied, but stayed within the error range from field of view distortion from camera lens. Angle β on the other hand behaved in a repeatable oscillation from cycle to cycle, but the noisier pattern shown for free moving endopodite portion of the paddle for this case Re 50, would change at other different Re condition.

3.4.2 The study of 4- paddle interaction for with and without metachronal paddling.

Metachronal paddling is defined where each paddle moved in an out-of-phase-pace compared to each neighboring paddle. A quarter period (25% phase different) is commonly maintain between each pleopod to its neighboring pleopod [Zhang et al. (2014)]. In this study, 25% phase difference between each paddle was used as a metachronal paddling model which is then compared with a synchronous 0% phase difference. The result show in figure 7 compares the result between synchronous and metachronal paddling for Re 50.

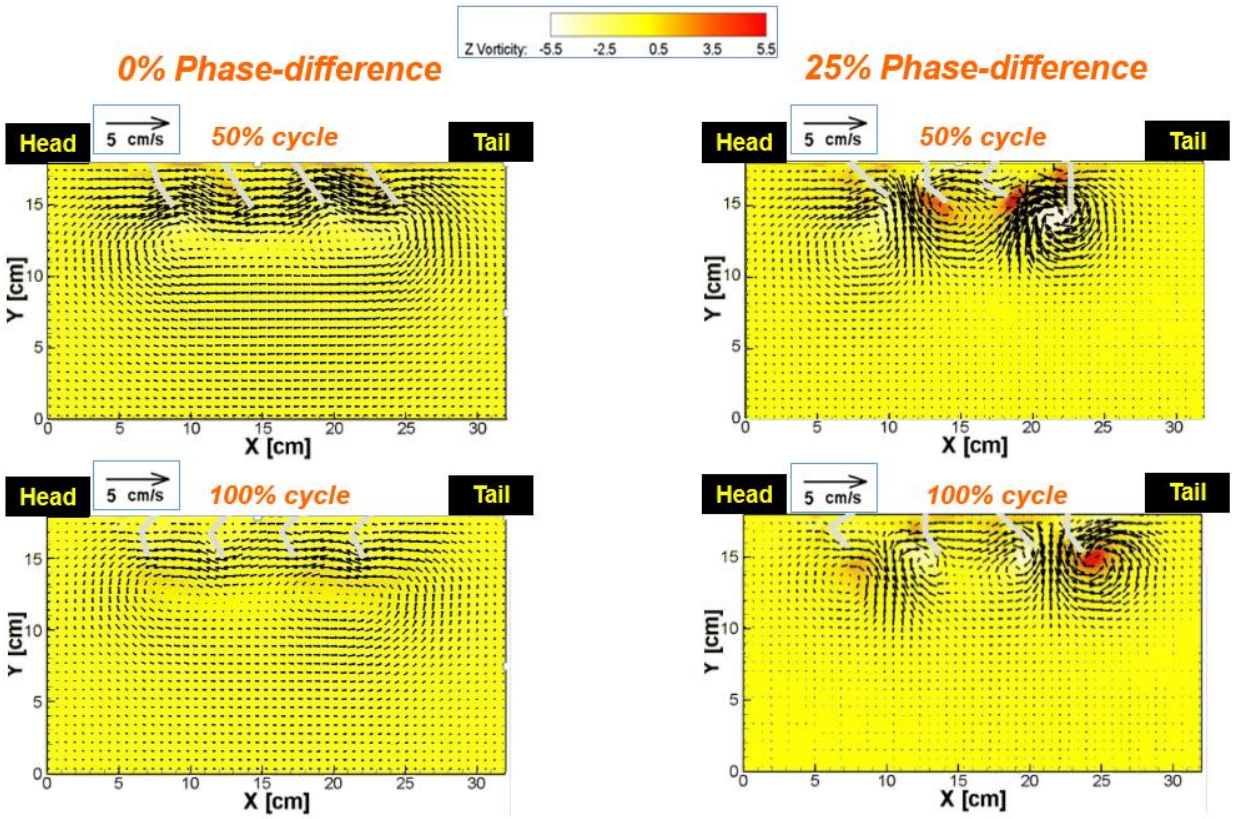

Figure 7 Result comparing synchronous and metachronal paddling motion of 4 hinged paddle structures in Re 50 conditions. Metachronal paddling of 25% phase difference shows more consistent backward flow at 50% cycle and 100% cycle due to the offset of power stroke stroke by 25% done by each individual hinged paddle. Synchronous paddling shows strong flow moving to the right during 50% cycle and flow moving to the left at 100% cycle which produce inefficient propulsion due to synchronous occilation motion.

From the result shown, it can be observed that in both cases of 0% and 25% phase difference, there is a net flow towards the back of the tail by looking at a stronger velocity vectors at 50% cycle (end of PS) then followed with a weaker return at 100% cycle (end of RS). The hinged paddle model with reduced surface area during RS, helped minimized the drag during RS. The main difference on metachronal paddling compared to synchronous motion was the consistency of back flow towards the tail throughout the cycle without a back and forth vector fields observed in synchronous paddling. As each of the paddle on the 25% phase difference case started PS at different time, there showed a more consistent pace of flow being pushed back towards the tail by individual paddle at every 25% cycle. As for the synchronous paddling with four paddle moving together, showed inefficient flow towards the back of the tail due to the pace of synchronous paddle that only starts a PS after every 100% cycle.

3.4.3 Looking at hydrodynamics of different Re number cases.

In order to get a better sense of hydrodynamics flow throughout metachrony cycle, processed plot showing velocity and vorticity were plotted at different point of a cycle (20%, 30%, 40%, 50%, 60%, 70%, 80%, & 90%) in figure 8. All three Re condition were plotted as well to look at the changes in flow interaction between inter-paddle as well as the wake. In each of this plot, PIV data were taken at the center of test section P_{V1} which can be referred to in figure 3. Comparison between each Re number at 100% cycle were shown in figure 9.

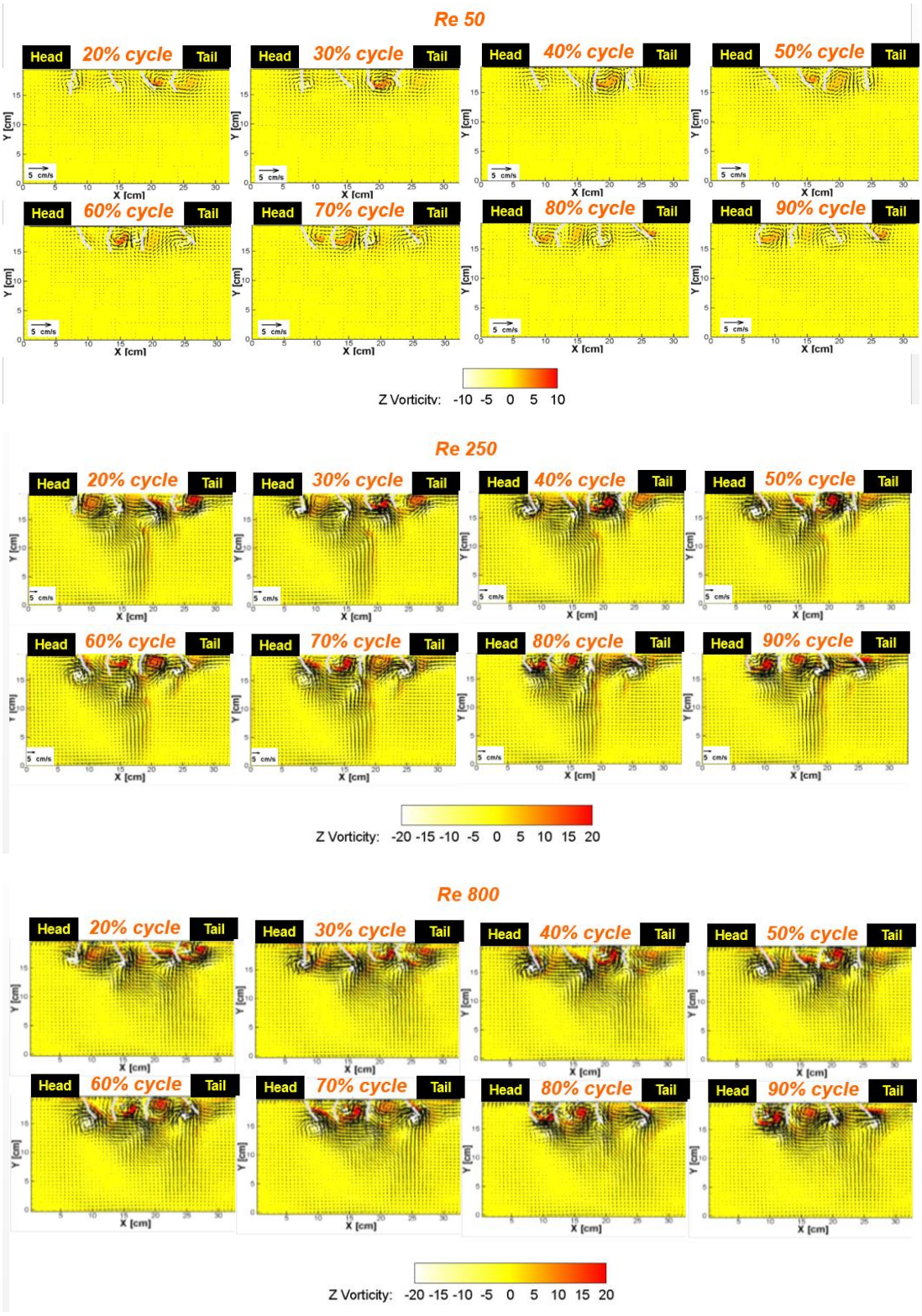

Figure 8 Plots showing 3 different Re condition at multiple points throughout a cycle. Stronger velocity field and vorticity contours were observed. The presences of vertical flow as Re increases were seen. Concentrated vortices were seen travelling from tail towards the head which suggests a tail to head wave motion.

The result in figure 8 showed interesting behaver of hydrodynamics flow during metachrony. Stronger vortices can be observed for all 3 Re cases concentrating at the 4th paddle at 20% cycle, and the vorticity concentration then traveled forward towards the 1st paddle as the cycle continues. For vortices travelling from back to front agreed with crustaceans' swimming style which is a tail to head wave motion, with the paddle closes to the tail starting PS sequence. The other observation from these plots was the presence of vertical flow as Re increases. In the case of Re 250, a more narrow and vertical generated flow was observed, and the flow started to propagate towards a wider and angled downward flow for the case of Re 800.

3.4.4 Looking at Re number changes in metachronal paddling from vertical PIV planes.

Crustacean animals with different sizes are able to swim around effectively with the same locomotion technique, metachronal paddling. This is an interesting topic to look into as how metachronal paddling is able to scale and function is vast range of sizes which in this study was tested with Reynolds number changes. In the result below, 3 different Re number of 50, 250, and 800 was chosen to compare the velocity vectors as well as vorticity contours created by metachronal paddling. For each Re number chosen, vertical PIV data from 3 different planes starting from the center of tank to 1.27 cm away from center plane and 3.81 cm away from center plane were shown in figure 9 to get a sense of the flow happening around the mechanism. The graph was plotted in terms of y (cm) vs x (cm) coordinates and its velocity vectors and vorticity contours are shown as well. All the example data shown in figure 9 were captured at 100% cycle [end of RS and start of PS for the next cycle for first paddle].

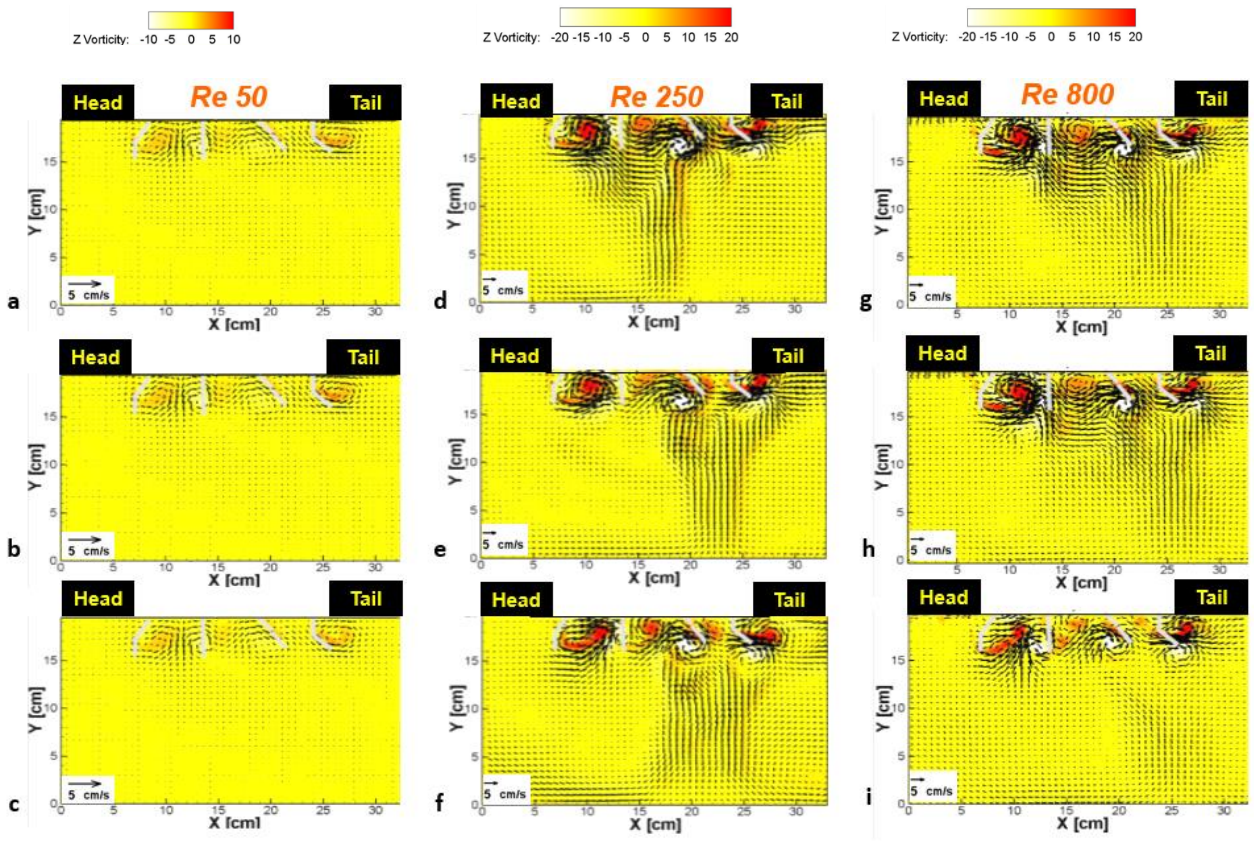

Figure 9 Reynolds number comparison of the same 25% metachronal paddling motion to study the effect of hydrodynamic flow around 4 hinged paddles. As the Re number increases, higher velocity vectors and vorticity contours were observed as well as the generation of downward flow. The downward producing flow shows widening effect as Re number increases which can be seen in the case of Re 250 with downward flow width around 2 paddle length and Re 800 case where the flow width expends to 3.5 paddle length. Flow hydrodynamics also shows slight reduce in magnitude as the data acquisition moves away from center plane (a to b to c) where a, b and c refers to PV,1, PV,2, PV,3 shown in figure 3.

By comparing the strength of the vorticity and vector field, Re 800 showed significant increase in velocity vectors comparing to Re 50. With the fluid that is less viscous as the Re number increases, more energy is able to transmit to the surrounding fluid hence registers a higher reading in velocity vector fields and vorticity contours. The next observation between the 3 Re cases was the present of angled downward flow at Re 250 and Re 800. Similar to observation in section 3.4.3, the downward flow also can be explained with lift generating flow occurred when Re number goes above the order of hundreds. As the Re number continued to increase, a more

concentrated downward flow (downward flow lasted 2 paddles gaps) started to expand and widens its lift band (downward flow starting from the 1st paddle and lasted for 3 paddle gaps or more) which produced a more angled wide downward flow. For Re 50 flow, velocity vectors and vorticity contours tend to stay closely surrounding the paddles with consistent patterns when acquired at different planes. Re 250 and Re 800 in another hand showed slightly weaker velocity fields and vorticity contours when moving away from the center plane and the overall backward flow seemed to maintain its dominants comparing to weaker lift flow when moving away from the center of test volume.

The next result acquired from this experiment was the horizontal velocity profile along the y axis. The velocity profile changes along height of the test volume gave us a good representation of horizontal flow magnitude propel towards the back of physical model. For consistency of result shown in figure 10, the velocity profile line for all cases were taken at the same reference x axis position which was one paddle length scale away shown in figure 10a (highlighted with a red vertical line). The comparison involved 3 Re cases of Re 50, 250 and 800 at 100% cycle. PIV data taken at multiple vertical planes which located at center plane, 1.37 cm away from center and 3.81 cm away from center were plotted to better visualize magnitude of velocity starting from the center of the tank and as the acquisition plane moved away from center plane. The plots were plotted with y (cm) vs dimensionless velocity (horizontal velocity at each y location relative to maximum horizontal velocity profile).

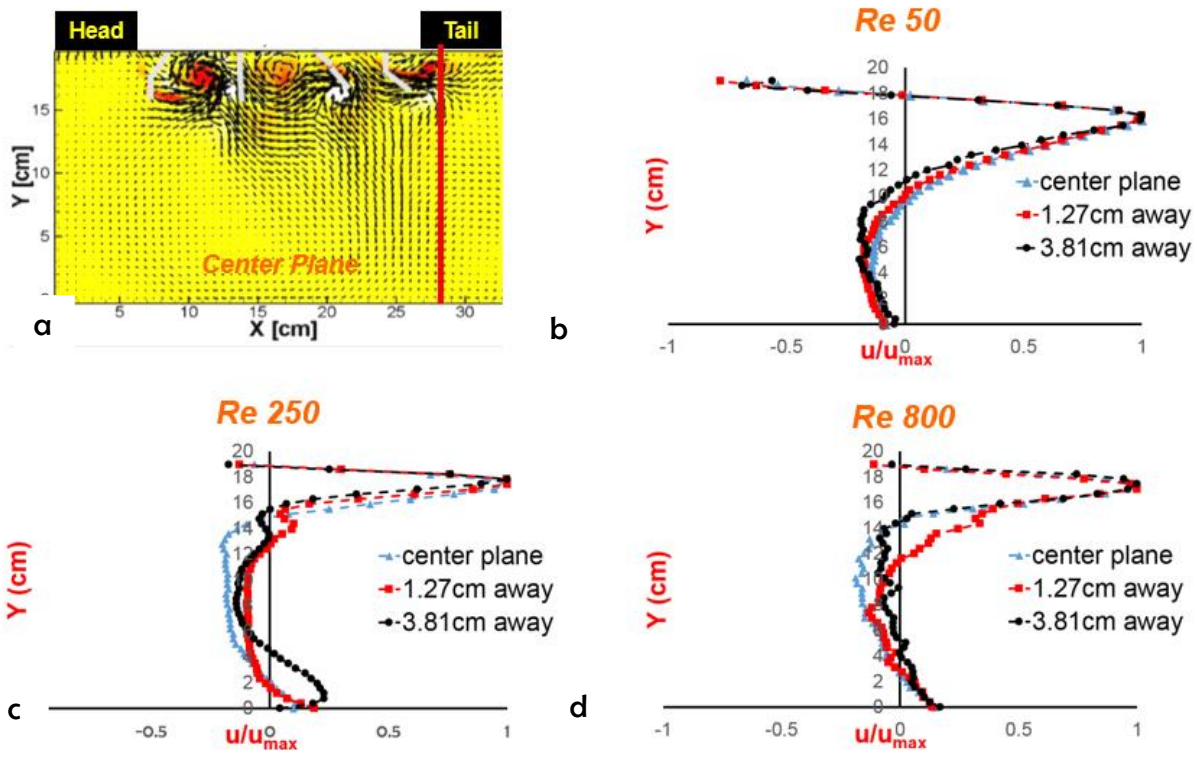

Figure 10 Horizontal velocity profiles were plotted at a constant position throughout different vertical PIV planes at 28cm (one paddle length away from 4th paddle). Each velocity vector points along the height (y axis) of each different planes were plotted in term of dimensionless u/umax where maximum horizontal velocity are different with different PIV planes. There is a larger range (10cm-18cm) of which the velocity profiles are positive for Re 50 case and a more narrow band for higher Re number case.

A clear observation from velocity profile comparison for all three Re cases were the higher horizontal flow pushed towards the tail of the physical model were located close to the paddle range above 15cm in the y axis. In all cases, the horizontal flow became weaker as the height moved lower and away from the paddle tip. There is present of negative flow towards the head of physical model around the mid-section of the test volume which can be seen for all 3 Re cases. Due to the present of angled downward flow seen in figure 8, the horizontal velocity profile at the mid-section of test volume is being absorbed into the downward flow channel. For all Re case in the order of 10 to 100, the velocity profile is strongest at the center of the test volume and weakens as the PIV plane moved away from the center. Even though the horizontal velocity

profile reduced as the plane shift away from the center PIV plane, the dimensionless velocity term relative to the local maximum horizontal velocity plotted to show similar trend above 15 cm. Therefore concluded that, the trend of horizontal velocity profiles are kept similar across of planes, even though the magnitude of horizontal velocity fields were slightly different.

The next plot was set up to look into vertical velocity (v_velocity) profile at different position in the test volume. Three heights within the test volume were chosen to extract the vertical velocity profile as a way to visualize the propagation of downward flow component. The three heights used in figure 11 were 5.04 cm, 10.16 cm and 15.24 cm below the paddle root. Re 50, Re 250 and Re 800 is being presented as an example for looking at lift propagation. The axis shown was vertical velocity verses the x coordinate acquired during PIV. The data plotted below were at the same time point as figure 10 which is at 100% cycle.

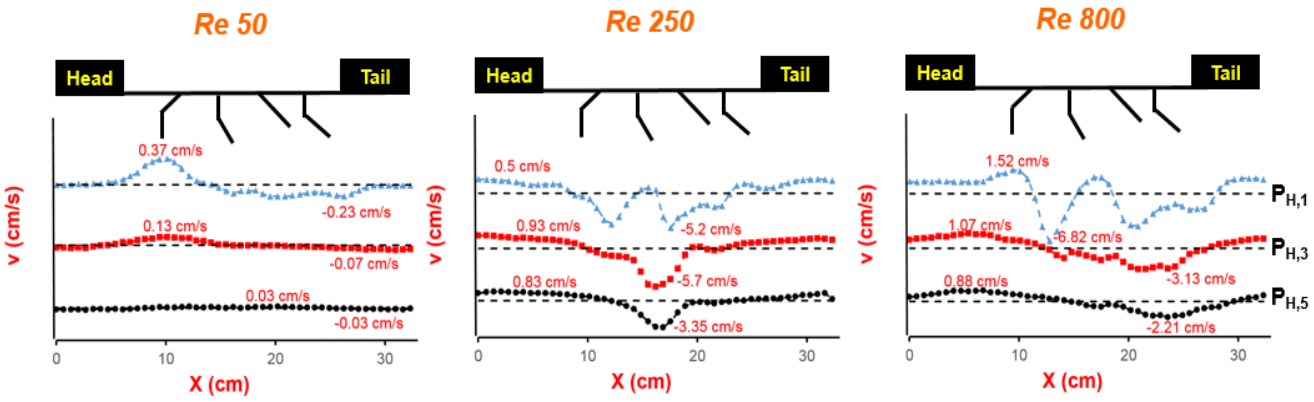

Figure 11 Vertical velocity profiles are plotted at different heights PH 1, 3 & 5 which can be referenced from figure 2. Due to more viscous fluid at lower Re numbers, vertical flow does not propagate depth wise of the test volume, whereas for Re 250 & Re 800 cases which showed downward velocity propagation through all 3 different horizontal planes which agrees with observation in figure 4. The downward flow for Re 250 propagated through 3 horizontal planes with a slight skewed to the right and Re 800 showed a larger skewness towards the tail of the body.

The first observation from figure 11 was the fluctuation of vertical velocities staying high closest to the paddle and weakens as it moved away from the paddling motion. For the paddling condition in Re 50, the fluctuation 5.04 cm away from the paddle root recorded a maximum magnitude of 0.37 cm/s upward flow as well as 0.23 cm/s downward flow. The fluctuation of vertical velocity then reduced for condition of height 10.16 cm below the paddle root with maximum of 0.13 cm/s upward flow and 0.07 downward flow. The lift component for Re 50 condition does not have enough thrust to propagate downward, therefore velocity profiles at 10.16 cm and 15.24 cm away from paddle root showed stable profile close to zero with minimal fluctuation. The other example of Re number in the hundreds showed stronger velocity fluctuation at all three heights comparing to Re 50. At 5.04 cm below the paddle root, 6.82 cm/s downward flow was registered for Re 800 case and 5.2 cm/s for Re 250 case which shows that there is a higher downward flow. The downward flow in higher Re number conditions was able to propagate lower in the test volume which can be seen for Re 800 example where a maximum downward velocity flow of 2.21 cm/s still can be observed 15.24 cm below the paddle root. The other observation for higher Re number condition was the slight angled downward vertical velocity flow concentrated at the 2rd and 3th paddle for Re 250 case and wider skewed downward flow towards the tail starting from 1st paddle all the way to 4th paddle for Re 800 which also agreed with the observation in figure 8.

The third step used to analyze vertical PIV planes was to calculate momentum flux for horizontal flow motion (flux in the x direction for swimming forward) and vertical flow motion (flux in the y direction for downward flow generation). The coefficient of thrust and lift were then calculated with the equations shown in section 3.3.5.4. Lift coefficient and thrust coefficient for Re cases of 50, 250 and 800 and the ratio between lift and thrust coefficient were plotted and shown in figure 12.

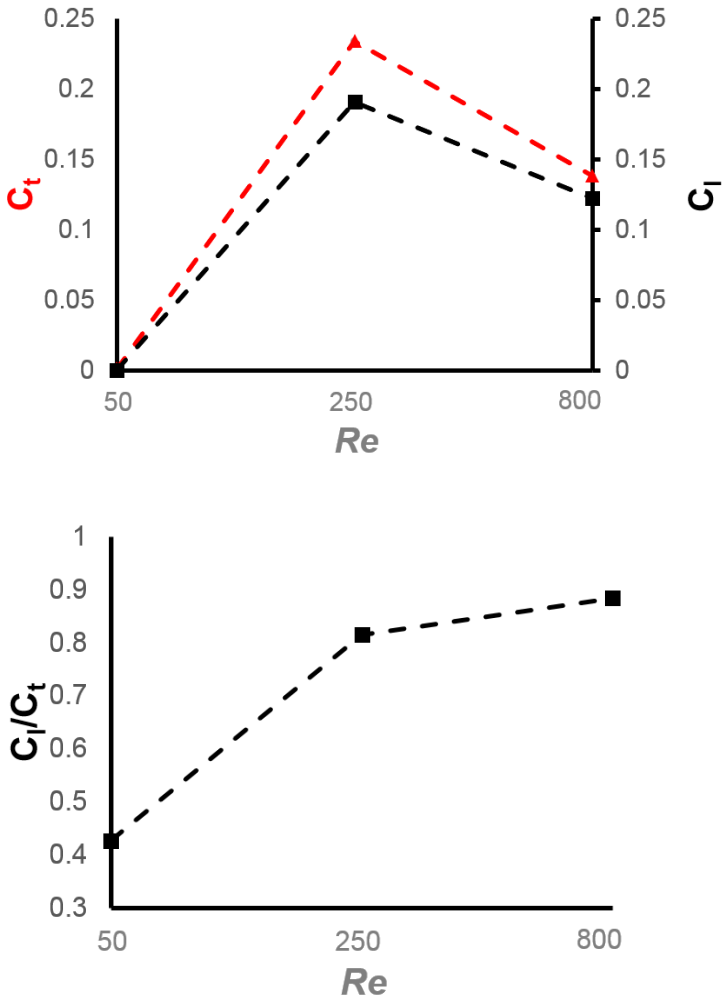

Figure 12 showed thrust and lift coefficient at different Re condition and also the ratio between lift and thrust coefficient.

From figure 12, lift and thrust coefficient showed highest at Re 250 and coefficient of thrust for all cases were more dominating compared to coefficient of lift. The difference between thrust and lift coefficient for Re 250 was larger compared to Re 800, hence the ratio of lift to thrust coefficient showed an increasing trend as Re condition increased.

3.5 Discussions

In this study, we built a four paddle physical model to achieve the goal of exploring the hydrodynamics of metachronal paddling. The kinematics of each artificial hinged paddle performed as expected with a generalized oscillation close to 25% phase difference. The lower part of the hinged paddle that were designed to be a free-moving portion (similar to endopodite) moved with a path that is repeatable, but the path changed slightly with different Re. The lower part of hinged paddle is designed to bend freely during recovery stroke, therefore different viscosity of fluid condition will affect the path motion. The next comparison done in this study was to look at hydrodynamics difference between synchronous and metachrony. The result showed a stronger net flow towards the tail of the physical model during PS and weaker return during RS in the case for metachrony. The sequential beating of PS from tail to head with the paddle closes to the tail starting PS and followed by the next PS from neighboring paddle, provides a more consistent net flow towards the tail. This study also looked at the scalability of metachronal paddling that simulates size variation experienced by tip of pleopod structures. Three Re of 50, 250, and 800 conditions were used and the result showed significant increase in magnitude of velocity vectors and vorticity contours at higher Re. The increase in Re condition alter the hydrodynamics wake from mainly horizontal flow to the generation of vertical flow. To quantify the vertical jet observation, momentum flux calculation is used to obtain the percentage of vertical flow generated by the inter-pleopod interaction during metachronal paddling. With the information of momentum flux components, we can then calculate lift and thrust coefficients. The result showed highest thrust and lift coefficient for the case of Re 250 and lowest at Re 50. Regardless of higher coefficients at Re 250, the difference between both coefficients were larger, therefore resulting in a smaller lift to thrust coefficient ratio. The plot for lift over thrust coefficient ratio showed an increasing tread as Re condition increases, and the result agreed with the hypothesis where more vertical flow should be generated for larger negatively buoyant body.

The contribution of metachronal paddling done by many studies today, broaden the understanding of such complicated locomotion system. Some studies done by [Murphy et al. (2013)], [Catton et al. (2011)] looked into in-vivo aspect of hydrodynamics generated wake. The observation from in vivo studies showed generation of downward flow for larger body similar to result shown on physical model. Experimenting with life animals, consistency of animal behavior and focus of view during recording are hard to achieve. One paper from [Lim et al. (2009)] done their experiments with combination of real-life body of lobster, but the motion of pleopods were controlled with programmable motors. [Zhang et al. (2014)], [Alben et al. (2010)], [Daisuke Takagi (2015)] studied metachronal paddling mainly with 2-dimensional computational modeling. Inter-pleopod interactions were discussed in computation model studies, but only rigid paddle were modeled with metachrony due to great challenge with designing real-life mimicking pleopod. Unlike previous work on metachronal paddling, our physical model addressed few of the challenges. Hinged paddle on physical model completes PS and RS characteristic similar to real-life pleopods, and metachronal paddling motion was tested in an ideal controlled condition. With high resolution PIV videos, inter-paddle synergistic interactions were clearly observed in our experiment which provides an advantage over in vivo studies. With the combination of hinged paddle structures and multiple runs with different Re conditions, scalability of metachronal paddling can be modeled and test. The bridged between the challenges of in vivo and computational module provides value to physical model studies.

3.5.1 Important of interaction between paddles

In section 3.4.2 of result section, synchronous and metachrony was discussed to highlight the advantages of metachronal wave motion. In the study done by [Murphy et al. (2013)] and [Alben et al. (2010)] phase difference was an important factor for crustacean with 4 to 5 pairs of pleopod structures. The optimum phase differences between ploepods are observed to be close to 20% for the case of 5 pleopods. Ideally for a 5 pleopod crustacean should spread out their individual PS

sequence from 100% oscillation stroke amplitude by the number of pleopod pairs which resulting to 20% each. The kinematics profile on physical model with 4 hinged paddles was set close to 25% phase difference and the divided phase sequence agrees with [Zhang et al. (2014)] computational module which said to be most efficient.

Inter-paddle synergistic interaction plays an important role in metachronal paddling with vorticity concentration from tail to head seen in section 3.4.3, yet net flow was transferred towards the tail direction. To explain how paddle interaction helps with producing vertical downward flow observed in result section, referencing similar to clap and fling [Birch et al. (2001)] [SP. Sane (2003)] can be used to explain the phenomenon.

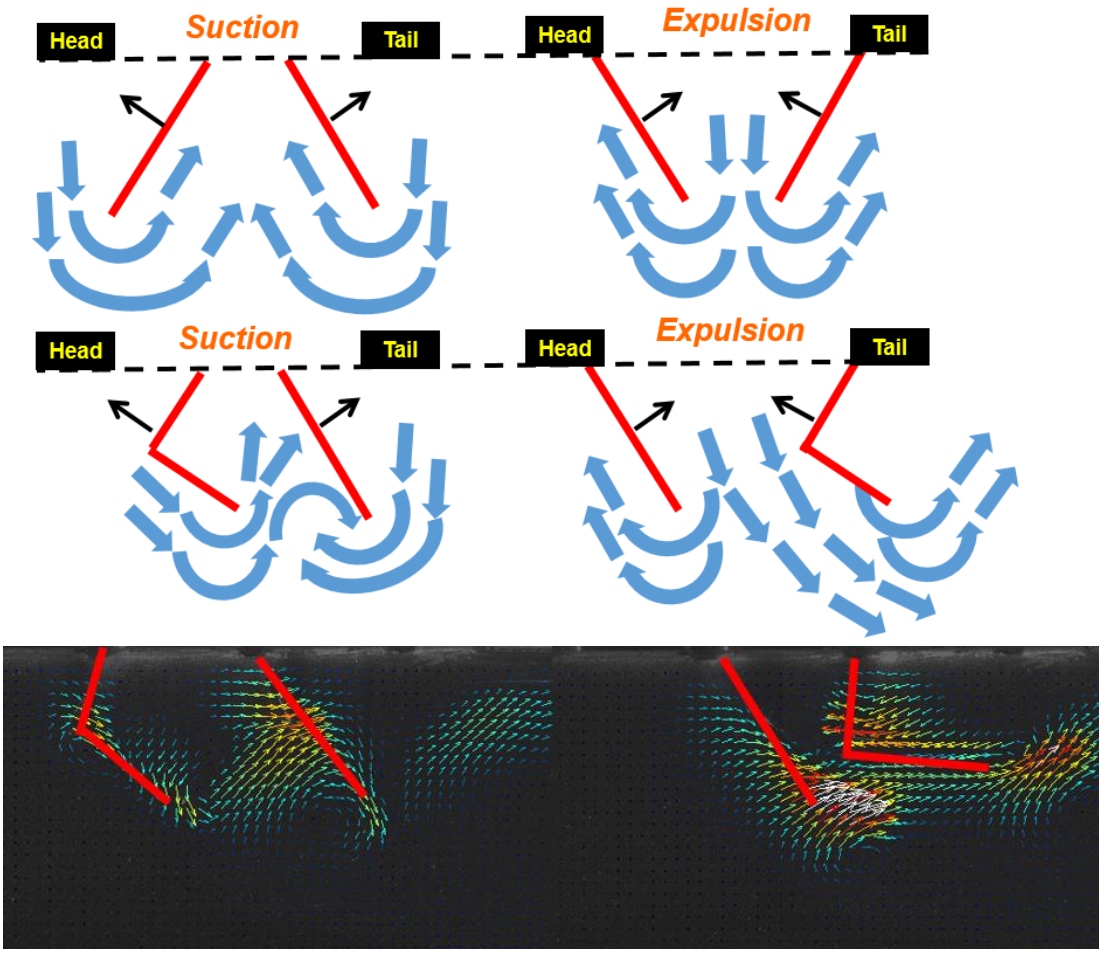

Figure 13 Schematic of paddle interaction relates to the idea of clap and fling. The figure explains the idea of suction and expulsion during metachronal phase difference with and without hinged paddle

From figure 13, the suction and ejection of fluid is mainly in the vertical axis symmetrically for a rigid clap and fling case. During the process of fling (left paddle RS and right paddle PS), vorticity flow is being draw in between both paddles. Flow is then push outward away from both paddle during clap (left paddle PS and right paddle RS). In the next case of using hinged paddle for clap and fling process, the flow can be observed to skew towards the tail. During the process of clapping, the hinged paddle on the right bends to allow more flow to escape towards the right. This combination of bend paddle and left paddle which is under PS provides an extra push of fluid towards the tail. The processed video for two paddle (7.62 cm total length) case study was done to illustrate the inter-paddle interaction. Due to thicker viscosity fluid condition in this case study as well as the absent of 4 complete hinged paddle, the downward flow component does not have enough strength to transfer through the depth of tank. The observation on downward flow can be seen in result section 3.4.3.

3.5.2 Re dependence of bulk flow patterns

The scalability of metachronal paddling for wide range of Re is being tested in this paper to understand in depth how similar locomotion style can work across different sizes ranging from less than 10 mm for Copepods to 236 mm for American lobsters [Lim et al. (2009)]. As Re increases from order of 10 to 100, vertical flow was observed. Momentum flux calculation for all 3 cases of Re showed increasing percentage of downward vertical component from 25% to nearly 50%. To bring it in perspective, large adult size crustacean at Re800 expends nearly half of its energy during swimming forward to downward flow. With the same paddling phase difference and frequency, the effect of suction and ejection of flow within inter-paddle should still remain valid as shown in figure 13. The reason vertical flow became more profound at higher Re is related to viscosity of surrounding fluid. With equal force exert paddles during clapping interaction to form skewed jet was not seen in Re50, because the energy done by paddles were not strong enough to propagate depth wise in the test volume. With weaker viscosity at Re 250

and 800 cases, stronger propagation of flow can be observed and the vertical band increased with increase of Re.

The effect of downward flow agrees with the observation of in vivo studies done by [Murphy et al. (2013)]. Metachronal paddling of hinged paddle moving in the direction of motion during PS and RS suggest a drag based locomotion, similar to rowing. Our physical model covered the range of Re condition from Re50 to Re800, which can be observed from krill species. This range of Re also shared similarities with other species for example, mysid shrimp (Re 64-125) [Hessler (1985)], copepods (Re 63-70) [Kohlhage (1994)] [Morris et al. (1990)] as well as adult lobster which operates at higher Re conditions [Lim et al. (2009)].

The physical model in this study provides us a leap forward in understanding of hydrodynamics from metachronal paddling with combination of realistic pleopod motion in controlled experimental condition. This model addresses the challenges in computational and in vivo studies. We can use this case study to introduce a new platform of physical model experiments on crustaceans, but there is more improvement for future work needed. Crustacean with smaller size like krill tends to have pleopod structures that are more flexible, while larger body like lobster embodied a more rigid pleopod structures. It would be good to introduced flexible paddle with interactable setae design on physical model. One of the limitations of this study was the tank confinement, and ideal place to test the physical model is in a large test volume where the metachrony wake does not feel a wall presence. Even though there is confinement in this study, but the observation of vertical flow and inter-paddle synergistic interaction were similar to in vivo and computational studies. The confinement of test volume will magnify the hydrodynamics of flow, but the comparison for different Re condition with the same test volume and experiment variables can still hold true. In the paper [Murphy et al. (2011)], discussed the other way of looking into size variation of crustacean species which was gap to length ratio of pleopods (0.2-0.65). In our study we used Re fluid condition variation to tackle size variation and the gap to

length ratio of physical model design was 1.33. The investigation of gap to length studies using a physical model have been investigated in upcoming publication.

In contrast to previous studies done by computational modeling and in vivo studies, our physical model achieved a better understanding in metachronal paddling by bridging the pros and challenges faced in previous study. In this study, metachrony of hinged paddle shown to be more effective compared to synchrony paddle in moving fluid towards the tail which agreed with computational model. The observation of vertical generated flow as Re increase behaved similar to in vivo studies of larger body sized animal as a way for them overcome negatively buoyant body. Besides similarities from previous studies, physical model experiment also added clear resolution on inter-paddle interaction and how metachronal paddle interaction helped with fluid movement. With the help of physical model platform, more studies on crustacean swimming can be added on in the future for example looking at how metachronal wave motion helps with krill schools, adding the number of pleopods structure and its phase difference to study how a system that is similar to ctenophores behave, and lastly contributing to future autonomous underwater vehicle AUV design.

CHAPTER IV

EFFECTS OF VARYING INTER-LIMB SPACING

4.1 Abstract

Crustacean aquatic animals for example krill, crayfish and shrimp ranging from youth to adult stage, spend most of their time swimming and staying afloat. The question on how metachronal paddling with a tail to head wave motion for a smaller body that is neutrally buoyant, sharing the same methods of locomotion compared to a negatively buoyant adult size body, is yet to be investigated thoroughly. The objective of this study is to build a physical model that is submergible in water-glycerin solution to study the propulsion system which typically consists of 4 to 5 pairs of pleopods. Regardless of large size variation in crustaceans, their pleopod to pleopod gap and pleopod length ratio stay within a tight range (0.2 to 0.65). The gap to length ratio G/L in this study were set with three gap plates to alter spacing between neighboring pleopod (2.54 cm, 3.04 cm, & 3.81 cm) while maintaining constant pleopod length (5.08 cm). Particle Imaging Velocimetry PIV techniques targeting center plane of 3D pleopod within test volume showed increasing velocity vectors and vorticity contours as Re increases. Decreasing of G/L ratio with constant Re showed improvement in synergistic interaction of metachrony. Stroke amplitude SA of each pleopod were shown to be limited to the geometry of each G/L ratio. With the study case of constant Re 250 and G/L = 0.6 while increasing SA (40deg, 60deg, & 80deg) showed improvement in percentage of horizontal flow from 84% to 94%.

4.2 Introduction

Crustacean such as lobster, crayfish, and brine shrimp employ large amount of time swimming and krill for example spend up to 73% of their total daily energy expenditure on swimming [Swadling et al. (2004)] [Kils (1981)]. Crustacean uses a unique swimming style known as metachronal paddling and is defined when pleopod structures move in an out-of-phase tail to head sequence with a delay period between one pleopod to the other [Knight-jones et al. (1959)]. This type of paddling motion which involves swimming pleopods to paddle in the direction of body movement suggests a drag-based propulsion system [JA Walker (2002)]. Studies from [Murphy et al. (2013)][Catton et al. (2011)] looked at crustaceans' metachrony from the perspective of in vivo studies, and the hydrodynamics of the wake and flow were mainly discussed. Due to the limitation of high resolution imaging and consistency from in vivo studies, synergistic interaction between pleopod to pleopod structures was not examined in detail. The uniqueness of metachronal paddling seen in crustaceans regardless for different size and weight, adapted to the same swimming style with closely paired pleopods for weight support and thrust have to be investigate further.

Studies have shown different sizes of crustacean operating in Reynolds number conditions between order of 10 to order of 1000 [Zhang et al. (2013)]. Re number experienced by each pleopods can be used as a way to relate the variation of size where smaller body will experience low Re and vice versa for larger size body experiencing higher Re. Recently [Murphy et al. (2011)] looked at another interesting way of scaling metachronal paddling which is the ratio of pleopod to pleopod gap and pleopod length. Instead of conventional way of Re around swimming body or pleopods, gap to length ratio can also affect the hydrodynamics of metachrony with its geometrical difference. Figure 14 will illustrate how gap and length of pleopods are defined in typical crustacean animal.

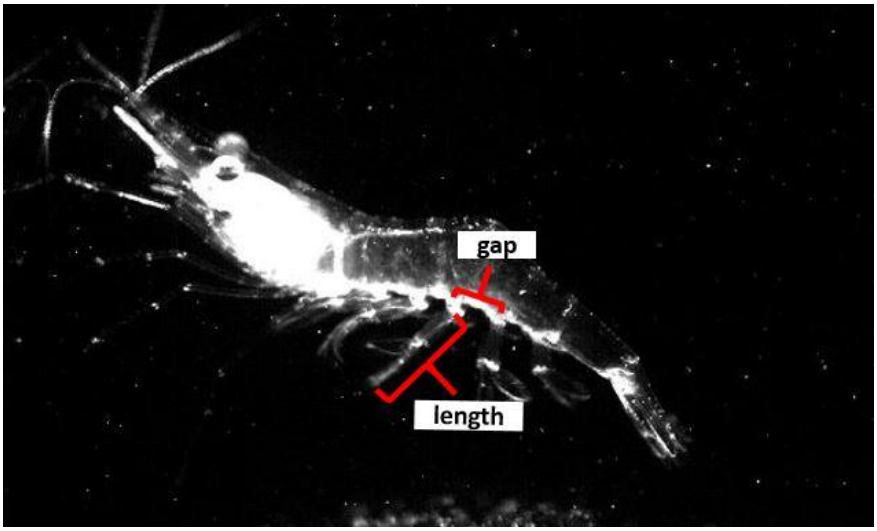

Figure 14 shows an acquired picture using a high speed camera of a ghost shrimp during metachrony. The figure also illustrate the definition of gap and length of each pleopod structures.

Regardless of different sizes of crustacean aquatic animals ranging from 1 mm for copepod to 226 mm for lobster [Lim et al. (2009)][Blaxter et al. (1998)] , the gap to length ratio of pleopods are surprisingly shown to stay within a tight range between 0.2 and 0.65 [Murphy et al. (2011)]. It is important to explore the significance of gap to length ratio in the context of hydrodynamics between closely packed pleopod structures. Stroke amplitude SA for one individual pleopod ideally should be able to oscillate for 180 degree, which is not the case for closely packed pleopod structures. SA of each pleopod in a group of pleopods are limited to the geometry introduced from G/L ratio. Therefore it would be interesting to look at hydrodynamics of flow generated from different G/L ratio of pleopod design and its capabilities from inter-related stroke amplitude.

The idea of using an idealized kinematics of each pleopod motion similar to in vivo observation and test the metachrony wave motion in different gap to length ratios will be valuable for understanding the hydrodynamics of crustacean swimming. In this study, we developed a physical model with four artificial pleopod-like structures that were electronically driven to

mimic metachronal paddling. 3 gap plates were introduced to the physical model to vary the gap of each pleopods with constant pleopod length in order to simulate different gap to length ratios. The physical model was placed in a tank containing water-glycerin mixture for dynamic scaling of Reynolds number. By implementing Re change in the order of 10 to order close to 1000 besides gap to length ratio, provides a more conclusive look at metachronal paddling. Our result shows the inter-pleopod jet interactions as well as the generation of downward jet similar to in vivo studies. Decreasing of G/L ratio and constant Re showed improvement in synergistic interaction of metachrony as the pleopods are closer to each other. Stroke amplitude SA of each pleopod were shown to be limited by the geometry set by each G/L ratio. With the study case of constant Re 250 and G/L = 0.6 while increasing SA (40deg, 60deg, & 80deg) showed improvement in percentage of horizontal flow from 84% to 94%

4.3 Methods

4.3.1 Physical Model

The 4 pleopod-like structures were closely design based on crustacean, that moves in an idealized back and forth motion with a 50% power stroke (PS) and 50% recovery stroke (RS) [Zhang et al. (2014)]. The PS moved in an opposite direction to the body's swimming direction which can also be explained with a head to tail motion, whereas in RS (tail to head motion) the paddle moved in the same direction as the swimming direction [Alben et al. (2010)]. The physical model for this study was setup throughout all experiments with PS starting from left to right which simulate the head on the left and tail on the right. The next challenge of modeling pleopod surface area change during PS and RS motion were addressed with implementation of hinged paddle design. Paddles were designed to expend to the max during PS to maximize drag surface area and bend during RS for the effectiveness of net flow toward the back of the body [Murphy et al. (2013)]. Each paddle consisted of two pieces of 2.54 cm length acrylic plate joint together with a hinge for a total of 5.08 cm length during PS.

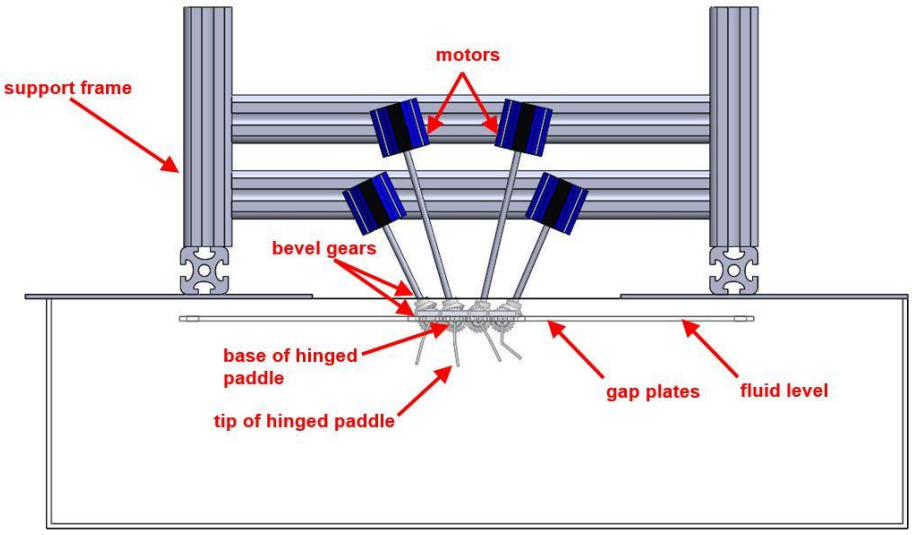

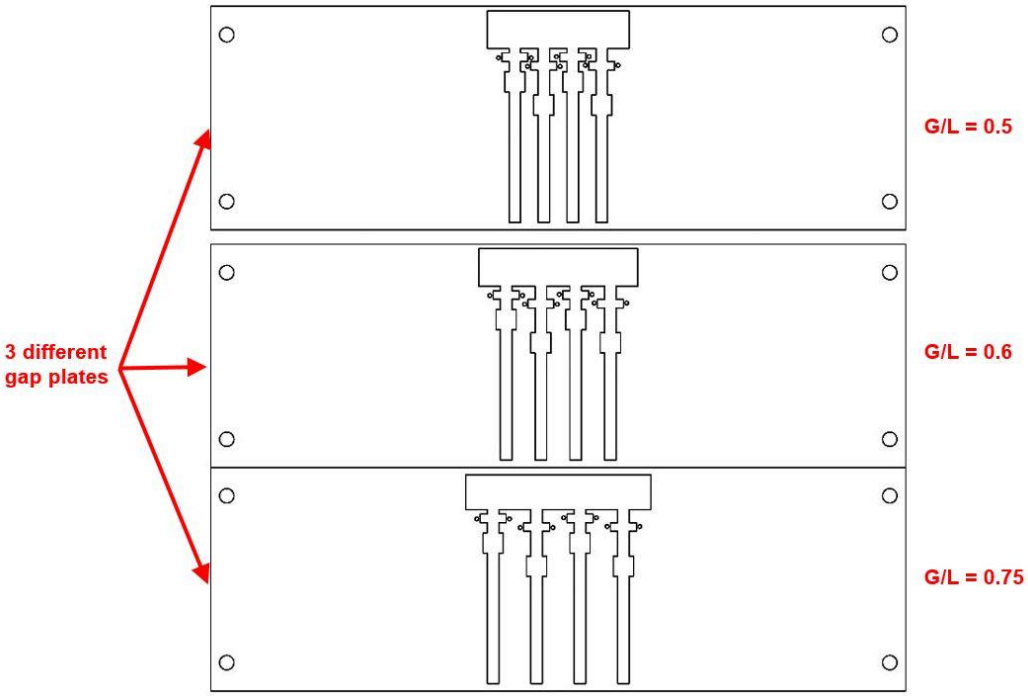

Figure 15 : Schematic of experimental physical model which consist of 3 major parts. (i) 12-gallon test aquarium, (ii) Four sets of programmable motor with shaft transmission, and (iii) 3 different gap plates for achieving gap to length ratio of (0.5, 0.6, and 0.75).

In order to achieve a repeatable oscillating motion, four programmable motors (ST23-4E, National Instrument, Austin TX, USA) were used for each paddle structure with its own motion profile. This combination allowed a total stroke amplitude of 60° with $\pm$30° motion referenced from center axis. The 60° stroke amplitude for this study was set based on the maximum stroke amplitude able for G/L ratio of 0.5 (pleopod to pleopod spacing of 2.54 cm and pleopod length of 5.08 cm). When four paddles move with an out-of-phase motion profile sequence determined from its starting position, metachronal paddling motion was demonstrated. Support frame (80/20 inc, Columbia city, IN, USA) was used to allocate four programmable motors at its needed position. Three paddle gap plates for housing each paddle were manufactured with acrylic material in order to alter the gap to length ratio (0.5, 0.6, & 0.75) needed in this study as shown in figure 15. Physical model assembly was mounted in a 45-liter glass tank (90 cm x 21 cm x 24 cm) (Mr. Aqua Co. Ltd, California, USA).

4.3.2 Gap to Length Ratio

In this study, the ratio of gap between each pleopod structures versus the length of pleopod was used to simulate size variation. In order to simplify the gap to length study, only one variable in the gap to length G/L term was altered. The only term that changed for each experiment was gap between each pleopod. The total length of all four paddles were set to a constant of 5.08 cm long, and the changing gap between each paddles were design to be 2.54 cm, 3.05 cm and 3.81cm.With this combination, produced a gap to length ratio study of 0.5, 0.6 and 0.75.

4.2.3 Reynolds number calculation and calibration

Reynolds number Re was changed in experiments to look at how gap to length ratio changes behave with different Re ranges. Water and glycerin mixtures were used to mimic different Re conditions experienced by pleopod. The Re formula used for calculation involved the amplitude (amp) of the angle of stroke experienced by the paddle tip at the maximum angular velocity. The reported formula was [$Re = \left(L_{leg}\right) * (L_{leg} * 2 * \pi * amp/T)/v$] (i) where paddle length (L_{leg}) as well as period of cycle (T) stayed constant on all experiment runs. Kinematic viscosity (v) was changed using multiple combination of water-glycerin solution. Multiple viscosity meter (100, 150, 200, 300, CANNON-FENSKE viscometer, CANNON Instrument company) were used to measure proper solution combination to meet required Re as shown in table 2.

v (cSt)	*Re*	% error *Re*
84	50	1.03
16.8	250	1.03
5.2	800	1.03

Table 2 Constant variables (i) The period of paddle oscillation was set to a constant of 2s, (ii) The paddle length was fixed at 5.08 cm, (iii) Hinged point was set to split the paddle in 50-50 ratio.

4.2.4 Kinematics

The main purpose of kinematics was to validate all four paddles kinematic motions on physical model. Alben et al. (2010) looked into the kinematics of krill with five pleopod, the phase difference of the upper haft of pleopod maintained close to 20% phase difference between each pleopod to the other. In the other study done by [Murphy et al. (2011)] showed similar phase difference for upper pleopod of a five pleopods E. superba. By referencing to [Zhang et al. (2014)] which worked on computational design on four 2D pleopod-like paddle, the paddle for physical model was set with an idealized motion profile of 25% phase difference. The physical model used in this paper was designed to run with metachrony close to 25% phase difference similar to Zhang's 4 paddle model due to the resulting total of 100% stroke cycle divided by number of paddles. In order to validate the motion on physical model, a custom Matlab code [T.L Hedrick (2008)] was used for two-dimensional tracking of high-speed videos. Information outputted with pixel by pixel coordinate of each tracked points can be converted to length scale and degree with careful calibration while recording. In each video frame, 8 points were tracked with 2 points on each of the four paddles [(1) midpoint between upper paddle (Protopodite) and lower paddle (Endopodite), (2) tip of paddle]. By using tracking point 1, the kinematics of the upper paddle was tracked and plotted.

4.2.5 PIV

Two-dimensional time-resolved particle image velocimetry (2D TR PIV) was used to visualized inter-pleopods flow and flow of the wake during metachronal paddling cycle. A schematic of the PIV experiment setup is shown in figure 16. Glass hollow spheres (110P8, LAVISION GMBH, Goettingen,Germany) were used as seeding particles inside the test volume. Vertical PIV plane ((P_{V1}) center plane of tank) was illuminated using a double pulse laser, single cavity Nd:YAG laser (Photonics Industry Inc., NY, USA) that provided a 0.5mm beam of 527nm in wavelength.

A cylindrical lens (10mm focal length) was used to make planer laser sheet from laser beam. A sCMOS0 camera (2600 x 2200 pixels, LAVISION Inc., Ypsilanti, Michigan, USA) was positioned in front of the physical model and focused on the seeding particles using a 60mm constant focal length lens (Nikon Micro Nikkor, Nikon Corporation, Tokyo, Japan). The aperture of camera lens was set on 2.8 for all experiment. A signal outputted from all 4 motors at the beginning of each cycle is linked with the programmable time unit (PTU) as a starting trigger in order to acquire data at the same starting point. The PIV particle size were in the range of 1.5-3 pixels. For each experiment, 20 raw PIV images per cycle were recorded with a camera frame rate of 10 frames per second. 50 cycles per experiment were taken with 5 sets of 10 cycle each due to the limitation of storing memory power. Particle displacements in the test volume ranged between 4-7 pixels. The physical model was allowed to run continuously for over 100 pleopod stroke cycle before acquisition of PIV data. Raw PIV images were processed using Davis 8.3.0 software (LaVision GmbH, Gottingen, Germany). The processed velocity vectors fields were averaged for 50 cycles. Multi-pass cross-correlation was performed on the PIV data with initial window size of 64x64 pixels (2 passes) to final window size of 32x32 (2 passes) with 50% overlap. Post-processing was performed by rejecting velocity vectors with peak ratio less than 1.2 and interpolation was used to replace empty vectors. Two dimensional velocity component (u in x direction, and v- in y direction) of flow in the test volume were obtained after PIV averaging.

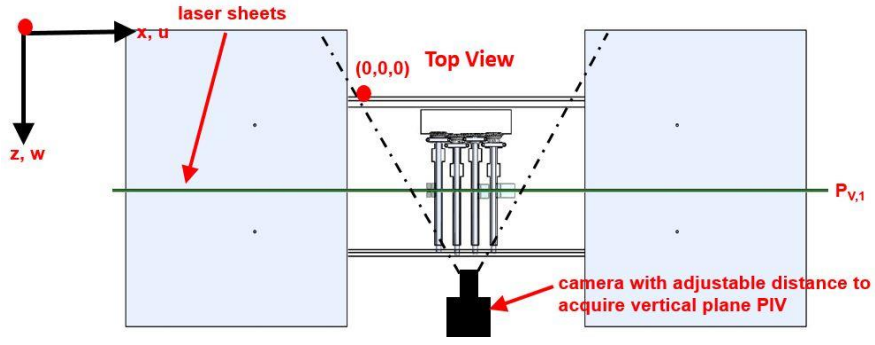

Figure 16 shows front and top view on where laser sheets plane are located during PIV acquisition. PV,1 represents vertical laser planes parallel to the front of the tank with location at center of the tank.

4.2.6 Definition of calculated quantities

4.2.6.1 Pleopods angle kinematics

Eight points were tracked on physical model in order to acquire coordinated change of each hinged paddle throughout a stroke cycle. The schematic of tracked point was showed in figure 17

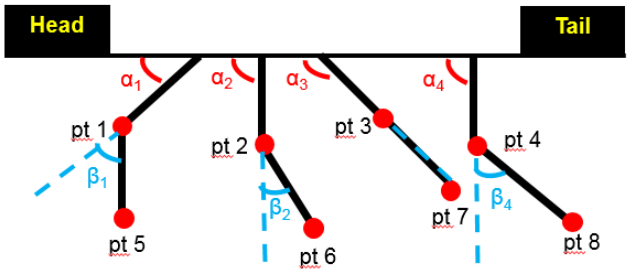

Figure 17 Kinematics references for tracking changes in angles throughout stroke cycle

The angles α and β can be obtained for a stroke cycle by using angle formula as defined:

$$\alpha_n = \tan^{-1}\left[\frac{(y(paddle_n\ root) - y(ptn))}{(x(paddle_n\ root) - x(ptn))}\right] for\ x(paddle_n\ root) > x(ptn) - - - (ii)$$

$$\alpha_n = 180 - \tan^{-1}\left[\frac{(y(paddle_n\ root) - y(ptn))}{(x(paddle_n\ root) - x(ptn))}\right] for\ x(paddle_n\ root) < x(ptn) - - - (iii)$$

$$\beta_n = 90 - \tan^{-1}\left[\frac{(y(ptn) - y(pt(n+4)}{(x(ptn) - x(pt(n+4)}\right] - - - (iv)$$

4.2.6.2 Vorticity

Out of plane z-vorticity, ω_Z was calculated using:

$$\omega_Z = \frac{\partial v}{\partial x} - \frac{\partial u}{\partial y} - - - (v)$$

4.2.6.3 Momentum Flux F_x &F_y

The momentum Flux calculation was set up as shown in figure 18. The left and right most boundaries were set at one paddle length scale away from the first and fourth paddle starting from left. The bottom boundary was set close to the bottom wall of the tank to capture the full effect of vertical flux.

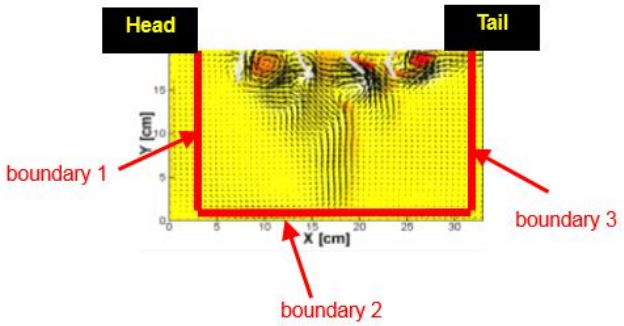

Figure 18 Momentum flux calculation boundaries were set up. Left and right boundaries were one length scale away from 1st and 4th paddle. The bottom boundary was set to be closest to the bottom of the tank.

With the boundaries set up, horizontal and vertical momentum flux can be calculated with the as shown below.

$$\frac{\partial}{\partial t}\int_{cv}\rho u\,dV + \int_{cs}\rho u(\vec{u}\cdot\hat{n})dy = \sum F_x \quad (vi)$$

$\frac{\partial}{\partial t}\int_{cv}\rho u\,dV \to 0$ time averaging

$$\sum F_x = \left[-\rho\sum_1 u^2dy\right] - \left[\rho\sum_2 uvdx\right] + \left[\rho\sum_3 u^2dy\right] \quad (vii)$$

$$\frac{\partial}{\partial t}\int_{cv}\rho v\,dV + \int_{cs}\rho v(\vec{u}\cdot\hat{n})dy = \sum F_y \quad (viii)$$

$\frac{\partial}{\partial t}\int_{cv}\rho v\,dV \to 0$ time averaging

$$\sum F_y = \left[-\rho\sum_1 uvdy\right] - \left[\rho\sum_2 v^2dy\right] + \left[\rho\sum_3 uvdy\right] \quad (ix)$$

4.4 Results

4.4.1 Kinematics of paddles on physical model.

Each paddle on physical model was recorded for 10 stroke cycles and was tracked to obtain kinematics using the equations from section 4.2.6.1. Eight points were tracked in each video with two points on each paddle [(i) hinged joint between upper pleopod and lower pleopod, (ii) tip of pleopod] shown in figure 17. The result of angle α and β were plotted as shown in figure 19.

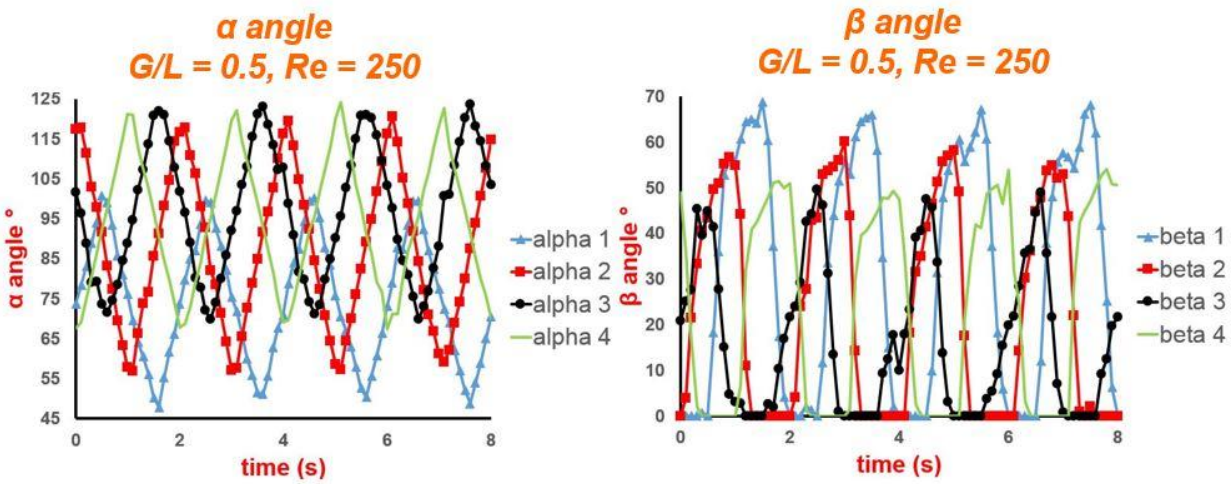

Figure 19 Kinematics from 4 stroke cycle were shown. Each α and β angle (paddle 1 closest to the head, paddle 4 closest to the tail) were plotted versus time. The kinematics of α angle for each paddle showed to be repeatable and close to 25% phase difference. B angle behaves in a noisier pattern and the kinematics will be different at each Re or G/L ratio cases.

The kinematics plot in figure 19 for angle α showed to be repeatable and close to 25% phase difference between one pleopod to the other. The degree range for each pleopod was slightly vary, but stayed within the error range of field of view distortion from camera lens. Angle β on the other hand behaves in a repeatable oscillation from cycle to cycle, but the noisier pattern shown on the plot for Re 50 case will not be the same at other Re and G/L conditions.

4.4.2 The study of synergistic interaction for constant Re and changing G/L ratio.

Metachronal paddling is defined where each paddle limb move in an out of phase pace compare to each neighboring paddle. A quarter period (25% phase different) is commonly maintain between each limb to its neighboring limb [Zhang et al. (2014)]. In this study, 25% phase difference between each paddle was used as a metachronal paddling model. The goal of this case study is to look at how synergistic interaction between each pleopod would react with changing the gap distance between neighboring pleopod. The G/L ratio result shown in figure 20 consisted of G/L ratio of 0.5 and 0.75 while maintaining Re of 250.

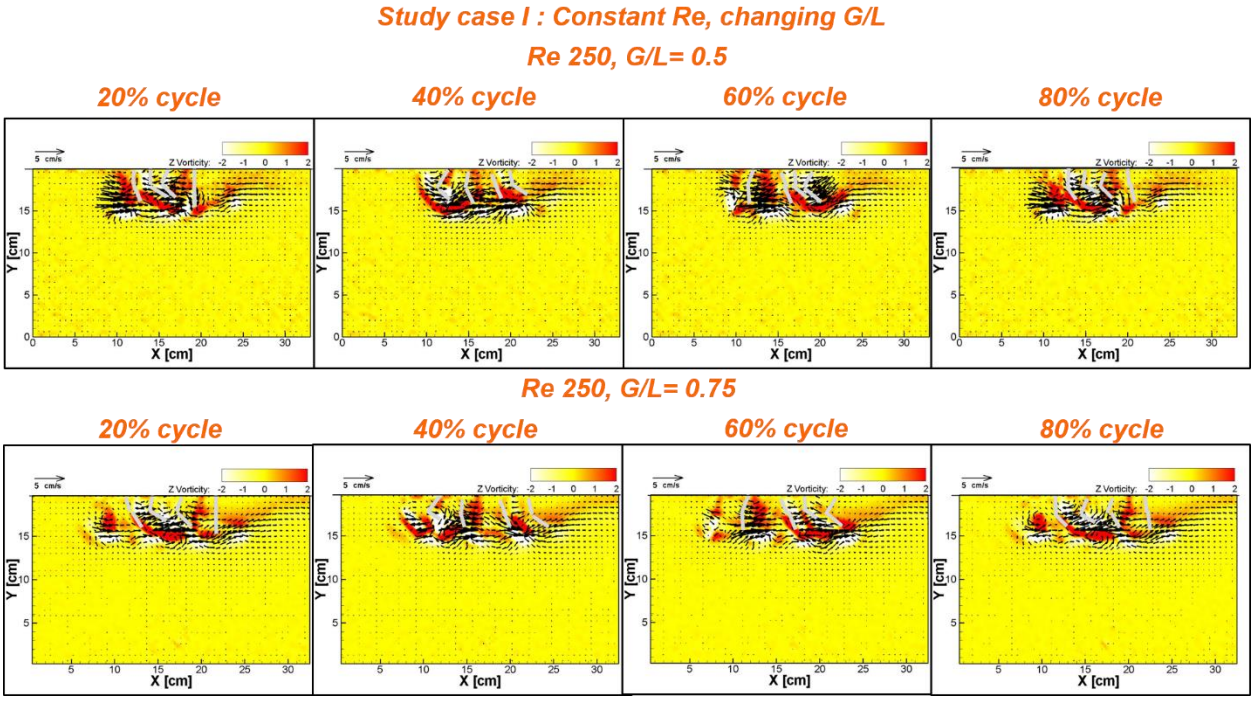

Figure 20 Result shown above consisted of velocity vectors and vorticity contours to look into synergistic interaction of closely packed pleopod structures. Both cases was tested with constant Re of 250 while varying G/L ratio of 0.5 & 0.75. Observation from this two result showed a more closely packed vorticity concentration for G/L =0.5 and wider propagation band for G/L = 0.75.

The flow moving towards the tail of physical model (right side) for both cases was consistent throughout all percentages of cycle. For G/L ratio of 0.5 showed a closely tight vorticity contours close to the center while for G/L ratio of 0.75 showed a wider band of influence stretching from 5 cm to 33 cm in the test section. Once the observation shown with respect to G/L change, the next plot will quantify the vertical velocity profile for the same case. Figure 21 shows the vertical velocity profile along the x axis of test section at two different heights [(i) pleopod tip or 5 cm below pleopod base, and (ii) 10 cm below pleopod base]. In each of the case shown, y axis represents vertical velocity in the units of cm/s and x axis represent horizontal coordinate in unit of cm.

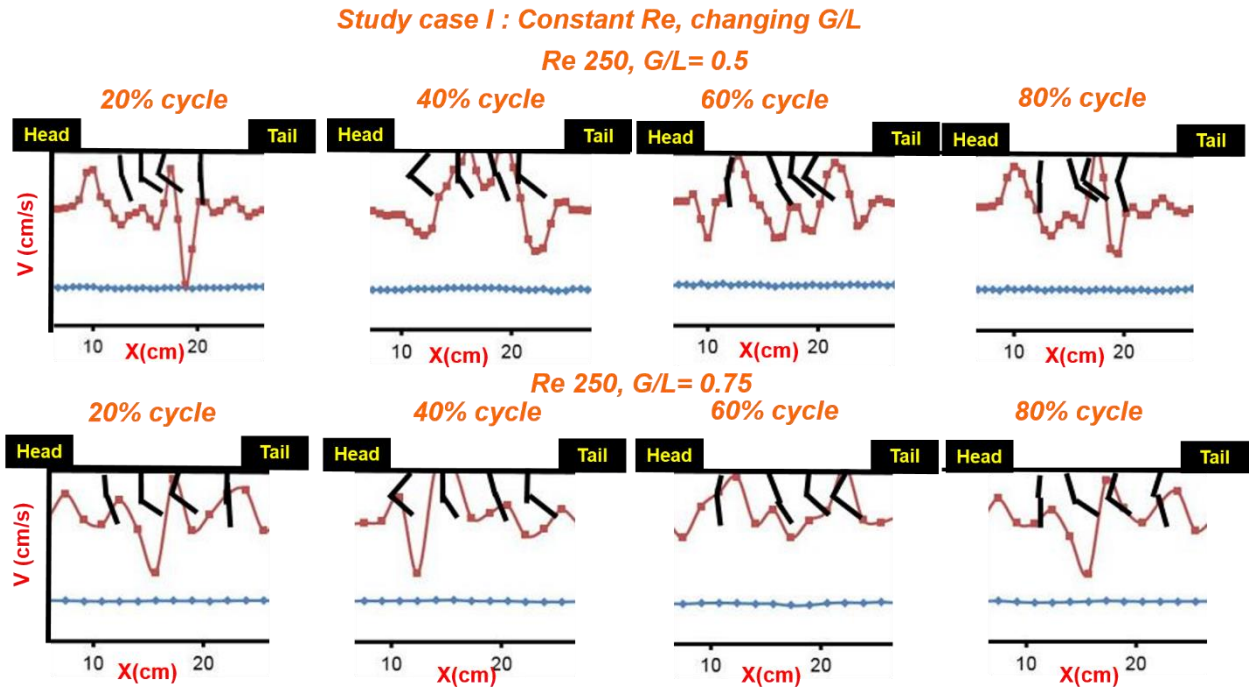

Figure 21 Plot shows vertical velocity profile with respect to G/L ratio change. Vertical velocity profile where plotted for two different heights [(i) tip of paddle or 5 cm below pleopod base, and (ii) 10 cm below pleopod base]. In both cases, vertical flow does not propagate downward through depth of test section. The vertical velocity plot at tip of paddle clearly shows synergistic interaction between paddles. In the case for G/L ratio of 0.5, maximum velocity of 1.77 cm/s upward flow and 1.94 cm/s downward flow were reported. 1.32 cm/s upward flow and downward flow were shown for G/L ratio of 0.75.

The vertical velocity plot in figure 21 suggested weaker propagation of flow depth-wise of test section for both G/L ratio cases. In contrast to flat line velocity profile at 10 cm below pleopod

base, high synergistic interaction between pleopod can be seen at 5 cm below pleopod base. In the case for G/L ratio of 0.5, maximum velocity of 1.77 cm/s upward flow and 1.94 cm/s downward flow were reported. 1.32 cm/s upward flow and downward flow were shown for G/L ratio of 0.75. Vertical velocity profile were observed to move upwards through physical model when pleopods opened up in fling, and flow pushed downward when pleopod structures come together in clap.

4.4.3 The study of synergistic interaction for constant G/L ratio and changing Re.

Besides looking at the effect of G/L ratio change, it was also the interest of this study to look at how Re number change with constant gap to length ratio affects the hydrodynamics of flow. In figure 22, velocity vectors and vorticity contours were plotted for the case where G/L ratio were maintained at 0.5 and Re change from order of 10 to order close to 1000.

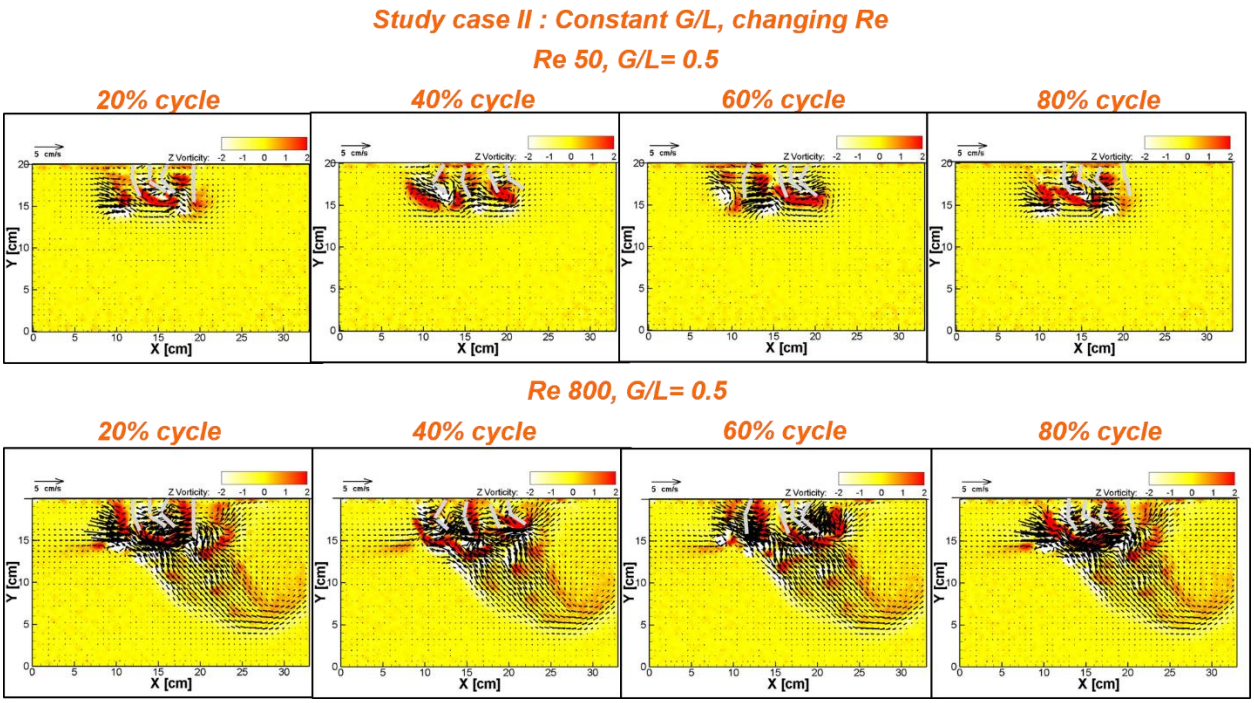

Figure 22 Plots showing velocity profile and vorticity contours for the case where G/L ratio were kept constant at 0.5 while altering Re number from Re 50 to Re 800. Vertical flow was observed for case with Re in the order close to 1000. The synergistic interaction between pleopods were stronger for Re 800 compared to Re 50.

The result in figure 22 with maintaining similar gap plates of 2.54 cm apart while changing Re number in the order of 10 to the order close to 1000, shown obvious vertical flow propagating depth-wise for Re 800. Stronger synergistic interaction were shown for higher Re case which also were repeatable through different percentage of cycle. Similar to figure21, the next plot shown was vertical velocity plot at two location similar to previous case study.

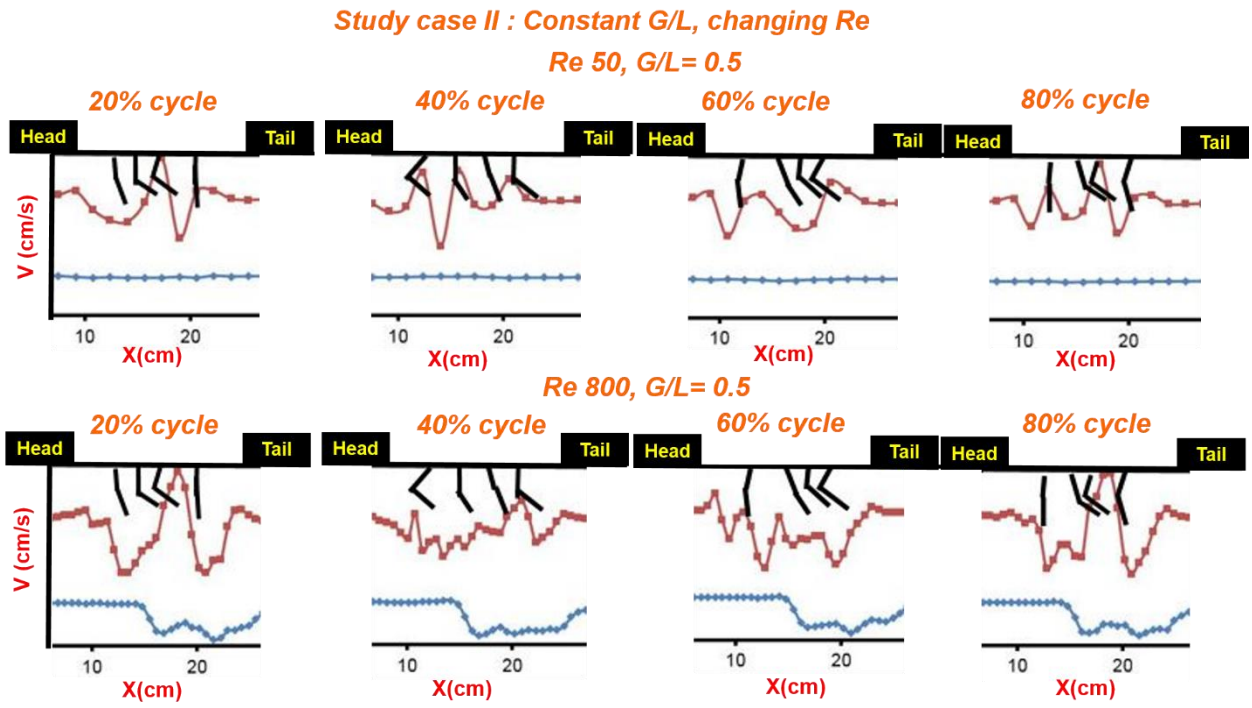

Figure 23 Plot shows vertical velocity profile with respect to Re change while retaining constant G/L ratio. Vertical velocity profile where plotted at two different heights [(i) tip of paddle or 5 cm below pleopod base, and (ii) 10 cm below pleopod base]. In both cases, vertical flow does not propagate downward through depth of test section. The vertical velocity plot at tip of paddle clearly shows synergistic interaction between paddles. For the case of Re 800, vertical flow propagation were shown at 10 cm below pleopod base with the maximum downward velocity of 1.71 cm/s. In the case for G/L ratio of 0.5 at height of pleopod height, maximum velocity of 1.06 cm/s upward flow and 1.21 cm/s downward flow were reported. 2.1 cm/s upward flow and 1.7 cm/s downward flow were shown for G/L ratio of 0.75.

The vertical velocity profile plot for figure 23 showed similar trend to figure 22 where vertical flow propagates downward through test section for Re 800 case. For the case of Re 800, vertical flow propagation was shown at 10 cm below pleopod base with the maximum downward velocity of 1.71 cm/s. In the case for G/L ratio of 0.5 at height of pleopod height, maximum velocity of

1.06 cm/s upward flow and 1.21 cm/s downward flow were reported. 2.1 cm/s upward flow and 1.7 cm/s downward flow were shown for G/L ratio of 0.75.

With vertical velocity profile shown to support the observation of downward propagation at higher Re number, it would be good as well to look at horizontal velocity profile. Dimensionless horizontal velocity profile was plotted at 100% of cycle located one paddle length scale away from the 4th paddle (right most pleopod closest to the tail similar to figure 10a). The y axis represents depth wise of test section and x axis represents horizontal velocity in the units of cm/s.

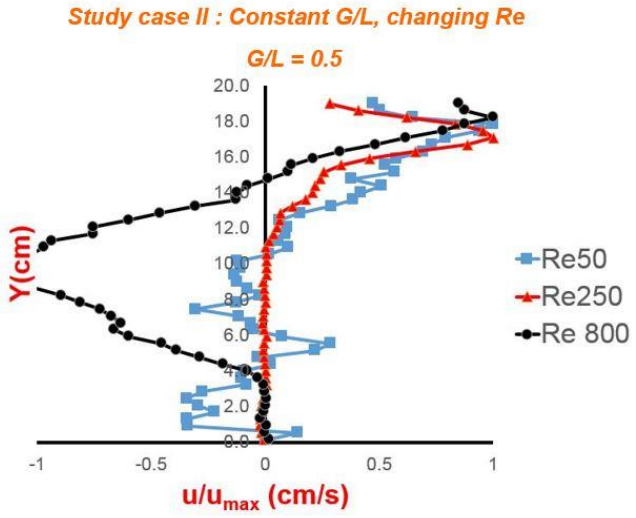

Figure 24 Dimensionless horizontal velocity profile were plotted at 100% cycle for constant G/L ratio while varying Re condition. Three Re number of 50,250, & 800 were plotted and horizontal velocity profile were acquired at one pleopod length scale away from the 4th pleopod structure (first pleopod counting from the right). Re 50 and Re 250 showed similar profile trend of positive horizontal flow at the top of test section which was closer to pleopod structures, and flow reduced to 0 as y axis travel downwards. Re 800 case stands out with large negative flow towards the left between y axis range of 4 cm to 14 cm which was due to the downward flow shown in figure 22.

Dimensionless horizontal velocity profile plotted at 100% cycle shows different trend for higher Re number of 800. Re 50 and Re 250 showed similar profile trend of positive horizontal flow at the top of test section which was closer to pleopod structures, and flow reduced to 0 as y axis travel downwards. Horizontal velocity flow for Re 50 was very low and close to 0.1 cm/s, therefore the dimensionless horizontal velocity profile was noisier compared to Re 250. Re 800 case stands out with large negative flow towards the left between y axis range of 4 cm to 14 cm

which was due to the downward flow shown in figure 22. When there is downward generating flow as shown for Re 800 case, flow from one paddle length scale away can be absorbed to the downward flow channel, hence resulting in negative horizontal velocity profile.

4.4.4 Significant of stroke amplitude in G/L ratio studies.

Stroke amplitude SA of each pleopod was closely related to different G/L ratio due to the limitation of geometry. 60 degree of stroke amplitude were set for this study based on the limitation of G/L ratio of 0.5 where the spacing between each pleopod was 2.54 cm. It would be interesting to expend this study by looking at effects of stroke amplitude change. G/L ratio of 0.6 (1.2 cm spacing between each pleopod) were chosen for this study with SA variation of 45deg, 60deg and 80deg. For simplification of this study, Re condition and gap plates were set to be constant.

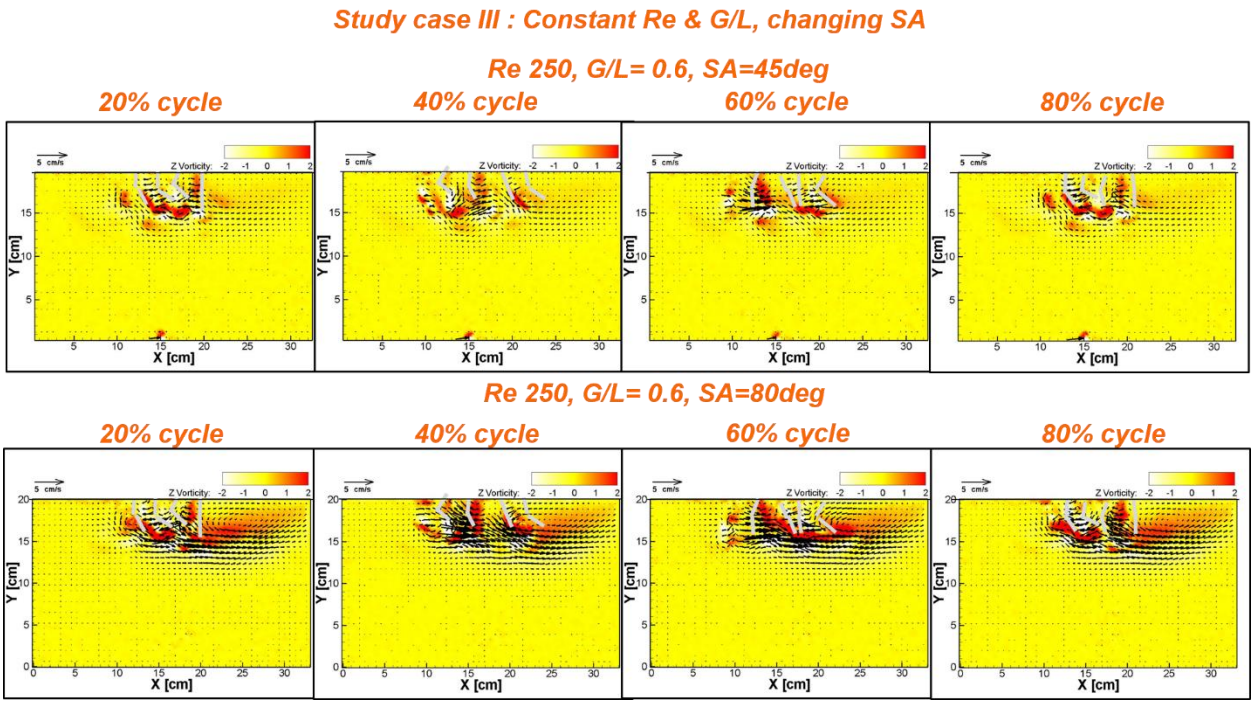

Figure 25 Plot showing effects of stroke amplitude SA change with constant Re condition and G/L ratio. Higher SA of 80deg showed stronger synergistic interaction of flow towards the tail of physical model. The band of vorticity height wise expended lower for SA 80 compared to SA 45.

Case study 3 with only varying stroke amplitude showed significant improvement in stronger velocity vectors and vorticity contours as SA increases to max amplitude. Higher SA of 80deg showed stronger synergistic interaction of flow towards the tail of physical model. The band of vorticity height wise expended lower for SA 80 compared to SA 45. Higher backflow towards the tail of physical model were observed as well as stroke amplitude were set to maximum stroke amplitude.

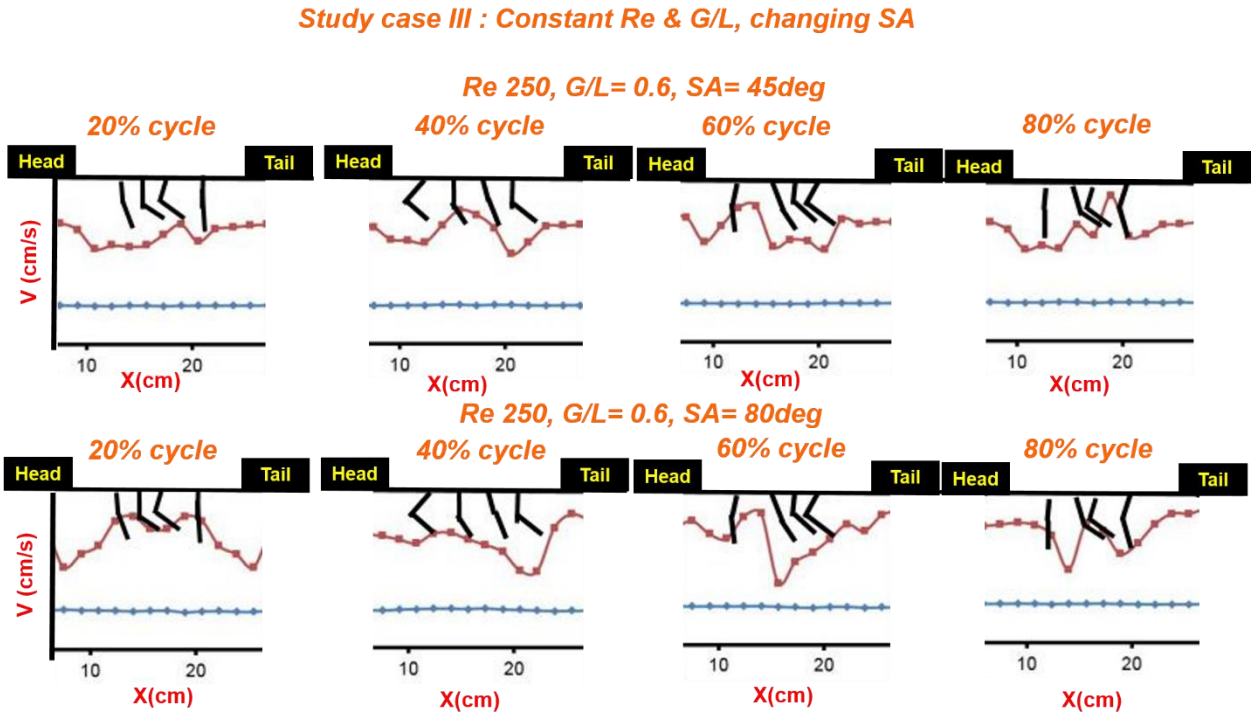

Figure 26 Plot showing vertical velocity profile for case where stroke amplitude SA was change while maintaining constant Re condition and G/L ratio. Increasing SA increases the power of vertical velocity profile with the help of greater synergistic interaction, but Re condition does not allowed propagation of flow downward.

Increasing SA showed in figure 25 increases the power of horizontal velocity profile with the help of greater synergistic interaction, but Re condition does not allowed propagation of flow downward. Maximum of 0.77 cm/s upward flow and 0.66 cm/s downward flow were shown for SA of 45deg, whereas 0.47 cm/s upward and 1.4 cm/s stronger downward flow was shown for SA

80deg. From figure 26, it can be seen that stronger flow for SA 80deg are mostly on horizontal flow and not propagated downward as shown here at 10 cm below pleopod base. To support the observation for figure 25 where horizontal flow were shown to magnify as SA increases but maintained the overall trend, dimensionless horizontal velocity profile plot were plotted. SA variation of 45deg, 60deg and 80deg tested with constant Re condition and G/L ratio.

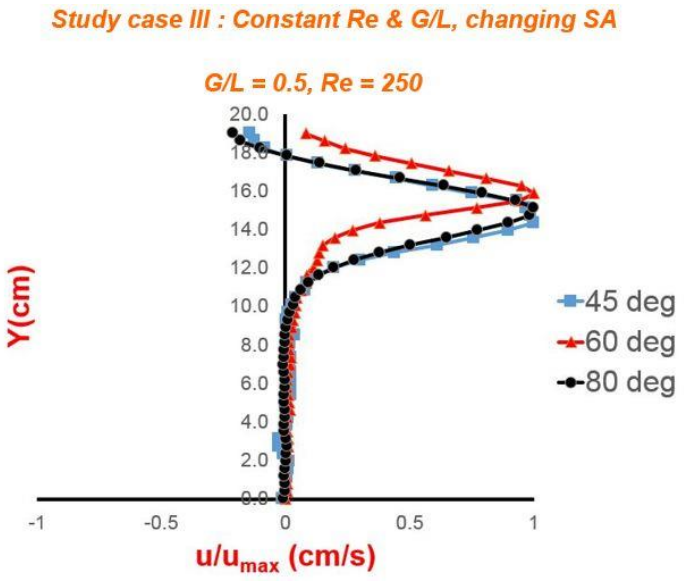

Figure 27 Dimensionless horizontal velocity profile were plotted for SA variation from 45deg, 60deg, and 80deg while maintaining constant Re condition and G/L ratio. All three stroke amplitude change showed similar trend in horizontal flow and flow propagation.

Dimensionless horizontal velocity profile plot for variation of SA while maintaining Re condition and G/L ratio showed similar trend and horizontal propagation. The magnitude of horizontal velocities were increase as SA increases as shown in figure 26, yet the increase in velocity magnitude does not affect the horizontal flow pattern.

4.4.5 Momentum flux calculation to quantify inter-relation of Re, G/L, & SA.

Next step used to analyze vertical PIV plane was to calculate momentum flux for horizontal flow motion (flux in the x direction) and vertical flow motion (flux in the y direction). The percentage of horizontal momentum flux relative to total flux generation from metachrony was shown in table 3.

	$\frac{\sum F_x}{\sum F_x + \sum F_y}$ [%]		
Re	G/L= 0.5	G/L= 0.6	G/L= 0.75
50	82.8	36.6	90.4
250	80	83.3	80.5
800	63.4	66.1	95.3

		$\frac{\sum F_x}{\sum F_x + \sum F_y}$ [%]
Re 250, G/L = 0.6	45deg	84.2
	60deg	83.3
	80deg	94.2

Table 3 Percentage of horizontal momentum flux were shown for all case study. The percentage of horizontal momentum flux showed to have an increasing trend for increasing G/L ratio for Re 800. The horizontal flow for Re 50 case were close to 0.1 cm/s (minimal flow propagation) therefore noisiness dimensionless horizontal velocity profile as shown in figure 11 effects the noisiness of Fx. Percentage of Fx shown to stay similar with increasing G/L ratio for Re 250. With increasing SA for constant Re condition and G/L ratio showed increasing in percentage of horizontal flux.

From table 3, the percentage of horizontal momentum flux showed to have an increasing trend for increasing G/L ratio for Re 800. The horizontal flow for Re 50 case were close to 0.1 cm/s (minimal flow propagation) therefore noisiness dimensionless horizontal velocity profile as shown in figure 24 effects the noisiness of Fx. Percentage of horizontal flux shown to stay similar with increasing G/L ratio for Re 250, but horizontal flow showed to increase from 63% to 95% for Re 800 case. With increasing SA for constant Re condition and G/L ratio showed increasing in percentage of horizontal momentum flux.

4.5 Discussion

In this study, we build a four pleopod physical model to achieve the goal of exploring the hydrodynamics of metachronal paddling. The kinematics of each artificial hinged paddle performed as expected with a generalized oscillation close to 25% phase difference. The lower part of the hinged pleopod moved with a path that is repeatable, but the path changed slightly with different Re. The lower part of hinged pleopod is designed to bend freely during recovery stroke, therefore different viscosity of fluid condition affects the path motion as shown in section 4.4.1 The first case was to look at the hydrodynamics of flow with changing G/L ratio while maintain Re condition. The result showed more horizontal propagation of flow with stronger vorticity contours. Depending on Re number range, the behavior of changing G/L ratio would be different. Re 800 showed increase in percentage of horizontal momentum flux from 63% to 95% as G/L ratio increases, whereas Re 250 showed similar range around 80% horizontal momentum flux as G/L increases. Both of this Re condition maintained constant stroke amplitude of 60deg which raises the question of how SA and G/L ratio works. When looking at constant G/L ratio and changing Re number, the velocity vectors and vorticity contours showed significant increase in magnitude for higher Re condition. The propagation of vertical velocity through the depth of test section was seen for Re 800 condition but not in cases of Re 50 or Re 250. This study suggested the importance of Re condition which played an effect on viscosity and hydrodynamic propagation done by pleopods. Now we know that Re condition, G/L ratio as well as stroke amplitude played an important role that relied on each other. The third case looked at only changing SA while setting Re condition and G/L ratio constant. The outcome for the example of Re 250 and G/L ratio of 0.6 with SA increment from 45deg, 60deg, to 80deg showed significant improvement in creating stronger synergistic interaction and flow being pushed towards the tail. Downward flow was not observed for this case due to Re condition even though metachrony was

ran at maximum stroke amplitude of 80deg. The percentage of horizontal momentum flux improved from 84% for SA= 45deg to 94% for SA= 80deg.

Re condition, gap to length ratio of pleopod design and stroke amplitude are all important inter-changing roles that will impact hydrodynamics of metachronal paddling.

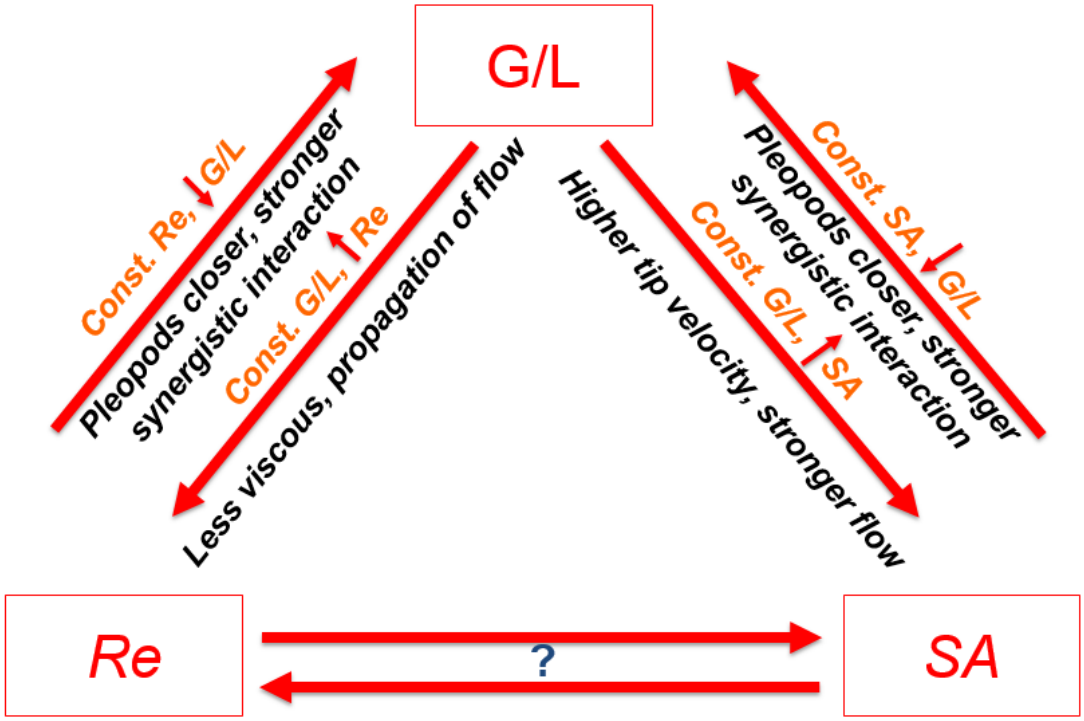

Figure 28 Chart showing importance of all three variables (Re condition, G/L ratio, & Stroke amplitude). All three terms played an important role in determining the hydrodynamics and synergistic interaction in metachronal paddling.

From the result acquired in the study for case Re 800, G/L ratio of 0.5 and SA of 60deg showed to have the strongest impact in synergistic interaction between all pleopods as well as the generation of vertical velocity propagation. Only if a case study fulfill all three positive relationships for each variable as shown in figure 28, improvement on hydrodynamics and a more pronounce synergistic interactions will be observe. For the case of Re 250 with changing G/L

ratio, Re condition played a role in preventing propagation of vertical velocity profile due to higher viscosity. SA of 60deg for G/L ratio of 0.5, 0.6 and 0.75 does not reached its maximum stroke amplitude of 80deg, therefore percentage of horizontal momentum flux was showed to maintain at 80% for all G/L runs. For the study done for increasing SA for constant Re250 and G/L of 0.6, stronger vorticity contours and momentum flux was shown as SA increases. Yet no vertical velocity propagation was seen because the study does not meet the positive requirement for higher Re number. In a nutshell, figure 28 provides an important relation for all three different changing variables that will impact the hydrodynamics of metachronal paddling. The relationships of between Re conditions and SA while maintaining constant G/L ratio for this study only looked at one case which was changing SA while setting Re at 250, more Re number have to be examine in the future to complete figure 28.

The contribution of metachronal paddling done by many studies today, broaden the understanding of such complicated locomotion system. Some studies done by [Murphy et al. (2013)], [Catton et al. (2011)] looked into in-vivo aspect of hydrodynamics generated wake. The observation from in vivo studies showed generation of downward flow for larger body similar to result shown on physical model. With life animal experiments, consistency of animal behavior and focus of view are hard to achieve. One paper from [Lim et al. (2009)] done their experiments with combination of real-life body of lobster, but the motion of pleopods were controlled with programmable motors. [Zhang et al. (2013)], [Alben et al. (2010)], [Daisuke Takagi (2015)] studied metachronal paddling mainly with 2-dimensional computational modeling. Inter-pleopod interactions were discussed in computation model studies, but only rigid paddle were modeled with metachrony due to great challenge with designing real-life mimicking pleopod. Unlike previous work on metachronal paddling, our physical model addressed few of the challenges. Hinged paddle on physical model completes PS and RS characteristic similar to real-life pleopods, and metachronal paddling motion was tested in an ideal controlled condition. With high resolution PIV videos,

inter-paddle synergistic interactions were clearly observed in our experiment which provides an advantage over in vivo studies. With the combination of hinged paddle structures and multiple combination runs of varying (Re condition, G/L ratio, Stroke amplitude), scalability of metachronal paddling can be modeled and test. The bridged between the challenges of in vivo and computational module provides value to physical model studies.

Inter-pleopod synergistic interaction plays an important role in metachronal paddling with tail to head motion, yet net flow was transferred towards the tail direction. To explain how paddle interaction helps with producing vertical downward flow observed in result section, referencing similar to clap and fling [Birch et al. (2001)] [SP. Sane (2003)] can be used to explain the phenomenon.

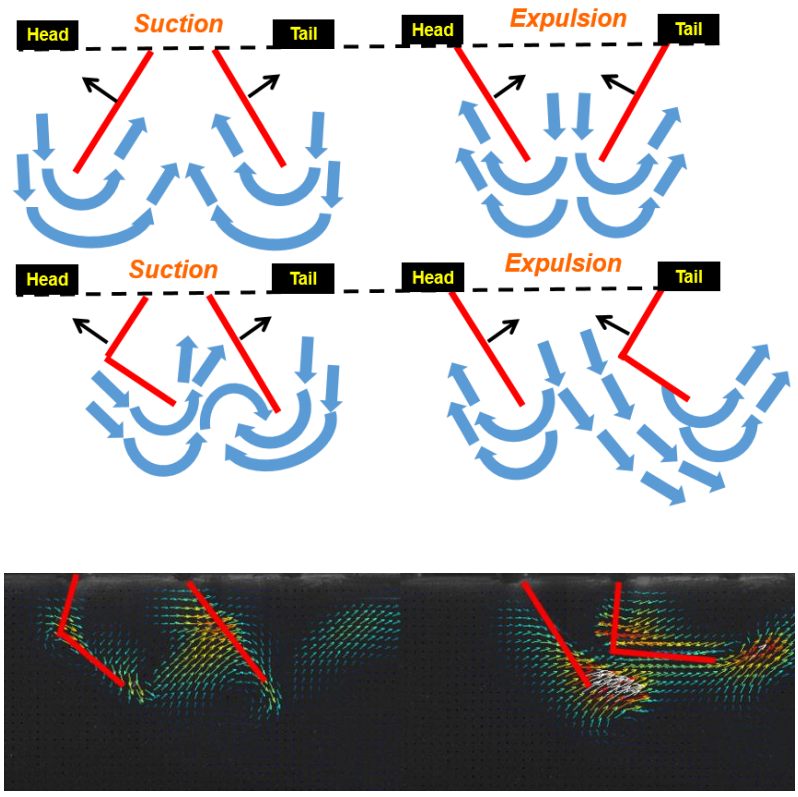

Figure 29 Schematic of paddle interaction relates to the idea of clap and fling. The figure explains the idea of suction and expulsion during metachronal phase difference with and without hinged paddle

From figure 29, the suction and ejection of fluid is mainly in the vertical axis symmetrical for a rigid clap and fling case. During the process of fling (left paddle RS and right paddle PS), vorticity flow is being draw in between both paddles. Flow is then push outward away from both paddle during clap (left paddle PS and right paddle RS). In the next case of using hinged paddle for clap and fling process, the flow can be observed to skew towards the tail. During the process of clapping, the hinged paddle on the right bends to allow more flow to escape towards the right. This combination of bend paddle and left paddle which is under PS provides an extra push of fluid towards the tail. The processed video for two paddle (7.62 cm total length) case study was done to illustrate the inter-paddle interaction.

The scalability of metachronal paddling is being tested in this paper to answer the question on why similar locomotion style can function across different sizes ranging from less than 10 mm for Copepods to 236 mm for American lobsters [Lim et al. (2009)]. As Re increases from order of 10 to order close to 1000, vertical flow was observed at Re 800 and G/L ratio of 0.5 with maximum SA. The effects of downward flow agree with the observation of in vivo studies done by [Murphy et al. (2013)]. Metachronal paddling of hinged paddle moving in the direction of motion during PS and RS suggest a drag-based locomotion, similar to rowing. Our physical model covered the range of Re condition from Re50 to Re800, which can be observed from krill species. This range of Re also shared similarities with other species for example, mysid shrimp (Re 64-125) [Hessler (1985)], copepods (Re 63-70) [Kohlhage (1994)] [Morris et al. (1990)] as well as adult lobster which operates at higher Re conditions [Lim et al. (2009)]. The other variable gap to length ratio used in this study for G/L of 0.5 and 0.6 stayed within typical crustacean range (0.2- 0.65). G/L ratio used for our study are closely similar to Pacific krill (G/L= 0.65), Northern krill (G/L= 0.48) and Remipedes (G/L= 0.3-0.52) [Murphy et al. (2011)]. The third G/L ratio used for our study of 0.75 is outside the range of typical species, yet it will be interesting to test the scalability of metachronal paddling model.

The physical model in this study provides us with a leap forward in understanding of hydrodynamics from metachronal paddling with combination of realistic pleopod motion in a controlled experimental condition. This model addresses the challenges in computational and in vivo studies. We used this case study to introduce a new platform of physical model experiments on crustacean and there is more improvement needed for future work. Crustacean with smaller size like krill tends to have pleopod structures that are more flexible, while larger body like lobster embodied a more rigid pleopod structure. It would be good to introduced free moving flexible pleopods on physical model. One of the limitations of this study was the tank confinement, and ideal place to test the physical model is a large test volume where the metachrony wake does not feel the presence of wall effect. Even though there is confinement in this study, the observation of vertical flow and inter-paddle synergistic interaction will still hold true. The confinement of test volume will magnify the hydrodynamic flow, but the comparison done in this study with consistent experiment setup and result comparison from previous studies should not discourage our findings. The other limitation of our study was the ability for our physical model design to explore lower ranges of gap to length close to the low range of 0.2. For future studies, introducing a changeable tail angle on physical model would be valuable as most crustaceans used their tail to divert flow direction from a more horizontal to vertical.

In contrast to previous studies done by computational modeling and in vivo studies, our physical model achieved a better understanding in metachronal paddling by bridging the pros and challenges faced in previous study. In this study, the importance of Re condition, gap to length ratio and stroke amplitude were shown to be inter-related to each other in order to maximize performance in metachrony. The observation of vertical generated flow as Re increase behaved similar to in vivo studies of larger body sized animal as a way for them overcome negatively buoyant body. Besides similarities from previous studies, physical model experiment also added clear resolution on inter-paddle interaction and how metachronal paddle interaction helped with

fluid movement. With the help of physical model platform, more studies on crustacean swimming can be added on in the future for example looking at how metachronal wave motion helps with krill schools, adding the number of pleopods structure and its phase difference to study how a system that is similar to ctenophores behaves, and lastly contributing to future autonomous underwater vehicle AUV design.

CHAPTER V

SUMMARY

5.1 Conclusion

Solving and improving next generation of autonomous underwater vehicle AUV were the main motivation of this study. AUV used today in search and rescue or exploration missions were typically costly and large in size. With its large size, maneuverability of AUVs was slow to response with large turn radius. Out of all disadvantages with AUVs design, the largest issue which this experiment study was designed to address is the single propeller propulsion system mostly used in AUVs today. The applications of AUV for such important search mission should not rely on only a single propeller which introduce high reliability issues that will compromise its mission if the only propulsion system fails. Besides reliability, the range of frequency for which the propeller rotates limits the operational Reynolds number range. Therefore a better solution to replace a single propulsion system was needed to start as a new platform for future generation of AUVs.

Best way to start is to look into bio inspired design from aquatic nature that have adapted to certain styles of swimming. Lift-based swimming for example tail undulation of fish or bell pulsation for jellyfish was considered for AUV design. With both designs either with a tail fin or a single pulsing bell do not improve the issue of single propulsion system in AUVs design. Adding to that, modelling an undulating tail motion or a pulsing bell require a whole new level of flexible-integrated design that would be more challenging. A more simplified version of propulsion system that improves current single propulsion design in required.

Crustacean aquatic animals for example, lobster, crayfish, and brine shrimp spend most of their daily energy usage on swimming and could be the ideal design for future AUVs. Crustaceans uses a unique swimming style known as metachronal paddling and is defined when pleopod structures move in an out-of-phase tail to head sequence with a delay period between one pleopod to the other [Knight-jones et al. (1959)]. Pleopod structures that are mostly rigid and consist of 4 to 5 pairs of pleopods that operates independently of each other provide an ideal model design for solving issues in current AUVs. The next question to validate metachronal paddling motion, as an alternate future propulsion system is the scalability of swimming model at different Re conditions and sizes.

In this study, we developed a physical model with four artificial pleopod-like structures that were electronically driven to mimic metachronal paddling. The physical model was placed in a tank containing water-glycerin mixture for dynamic scaling of Reynolds number. We first test the effect of synchronous paddling versus metachrony. The result showed significant improvement of flow being pushed towards the tail end in the case of metachronal paddling. The 25% phase lag used in our four pleopod physical model, provided a consistent scooping of flow towards the tail of model. The next experiment conducted, looked at how metachronal paddling motion scaled with different Re condition from the order of 10 to order close to 1000. Higher Re condition of Re 800 showed significant increase in velocity profiles and vorticity contours compared to Re 50

case. Vertical velocity flow was observed as Re condition increases, and the downward flow seems to undergo transition from vertical downward flow for Re 250 case to angled jet for Re 800. The observation of vertical flow for higher order of Re in metachrony with the same frequency and pleopod length can be explained with the synergistic interaction between pleopods. Flow managed to propagate downwards due to less viscous solution as Re increases. Momentum flux calculation done with cycle averaging showed increasing of percentage of vertical flow. The momentum flux components were used to calculate thrust and lift coefficients. The result showed highest thrust and lift coefficient for the case of Re 250 and lowest at Re 50. Regardless of higher coefficients at Re 250, the difference between both coefficients were larger, therefore resulting in a smaller lift to thrust coefficient ratio. The plot for lift over thrust coefficient ratio showed an increasing tread as Re condition increases, and the result agreed with the hypothesis where more vertical flow should be generated for larger negatively buoyant body.

The next case study looked at scalability of metachronal paddling in terms of the ratio of pleopod to pleopod gap to pleopod length. The gap to length ratio of pleopods across all crustacean species is surprisingly shown to stay within a tight range between 0.2 and 0.65 [Murphy et al. (2011)]. For our physical model studies, 3 gap plates were introduced to vary the gap of each pleopod with constant pleopod length, in order to simulate different gap to length ratios (G/L= 0.5, 0.6, 0.75). By implementing Re change in the order of 10 to order of 100 besides different gap to length ratios, provide a more conclusive look at metachronal paddling. Our result showed inter-pleopod jet interactions as well as the generation of downward jet similar to chapter 2. Reducing of G/L ratio (closer gap between pleopod neighbors) with constant Re showed improvement in synergistic interaction of metachrony. Stroke amplitude SA of each pleopod were shown to be limited by the geometry of each G/L ratio as the gap between each pleopod sets the maximum stroke amplitude. With the study case of constant Re 250 and G/L = 0.6 while varying SA (40deg, 60deg, and 80 deg) showed improvement in percentage of horizontal flow from 84%

to 94%. The reason for the increase of percentage of horizontal flow was due to the increase in tip velocity on each pleopod; with constant frequency of 0.5 Hz, SA of 80deg traveled greater distance for the same amount of time, hence higher tip velocities. The importance of inter-related relationships between Re condition, pleopod G/L ratio as well as stroke amplitude that on its own would affect the hydrodynamics of metachronal paddling were presented here in this study.

The result obtained from this paper creates a new platform for future AUVs design by altering the variables like pleopod G/L ratio, stroke amplitude as well as Re number experience from pleopod tip in order to successfully operate in vast range conditions. Of course there are more studies needed to be done to conclusively answer the behavior of metachrony swimming. Crustaceans with smaller size like krill tends to have pleopod structures that are more flexible, while larger body like lobster embodied a more rigid pleopod structure. It would be good to introduce free moving flexible pleopods on physical model. One of the limitation of this study was the tank confinement, and the ideal place to test the physical model is a large test volume where the metachrony wake does not feel the presence of wall effect. Even though there is confinement in this study, the observation of vertical flow and inter-pleopod synergistic interaction will still hold true. The confinement of test volume will magnify the hydrodynamic flow, but the comparison done in this study with consistent experimental setup and result comparison from previous studies should not discourage our findings. The other limitation of our study was the ability for our physical model design to explore lower ranges of gap to length close to the low range of 0.2.

With the help of physical model platform, more studies on crustacean swimming can be added on in the future, for example looking at how metachronal wave motion helps with krill schools. Adding the number of pleopods structure and playing with different phase difference should be interesting to look at. Lastly introducing of a changeable tail angle on physical model would be valuable as well, as most crustaceans used their tail to divert flow direction from a more horizontal to vertical

REFERENCES

.

1. Eriksen, Charles C., et al. "Seaglider: A long-range autonomous underwater vehicle for oceanographic research." IEEE Journal of oceanic Engineering26.4 (2001): 424-436.
2. Prestero, Timothy. Verification of a six-degree of freedom simulation model for the REMUS autonomous underwater vehicle. Diss. Massachusetts Institute of Technology and Woods Hole Oceanographic Institution, 2001.
3. Yoerger, Dana R., et al. "Techniques for deep sea near bottom survey using an autonomous underwater vehicle." The International Journal of Robotics Research 26.1 (2007): 41-54.
4. McGann, Conor, et al. "Preliminary results for model-based adaptive control of an autonomous underwater vehicle." Experimental Robotics. Springer Berlin Heidelberg, 2009.
5. Yoerger, Dana R., John G. Cooke, and J-JE Slotine. "The influence of thruster dynamics on underwater vehicle behavior and their incorporation into control system design." IEEE Journal of Oceanic Engineering 15.3 (1990): 167-178.
6. Alvarez, A., et al. "Folaga: A low-cost autonomous underwater vehicle combining glider and AUV capabilities." Ocean Engineering 36.1 (2009): 24-38.
7. Fish, Frank E. "Transitions from drag-based to lift-based propulsion in mammalian swimming." American Zoologist 36.6 (1996): 628-641.

8. Sfakiotakis, Michael, David M. Lane, and J. Bruce C. Davies. "Review of fish swimming modes for aquatic locomotion." IEEE Journal of oceanic engineering 24.2 (1999): 237-252.
9. Murphy, David W., et al. "Underwater flight by the planktonic sea butterfly."Journal of Experimental Biology 219.4 (2016): 535-543.
10. Larson, Mary, et al. "Effect of metachronal phasing on the pumping efficiency of oscillating plate arrays." Experiments in Fluids 55.5 (2014): 1-13.
11. Birch, James M., and Michael H. Dickinson. "Spanwise flow and the attachment of the leading-edge vortex on insect wings." Nature 412.6848 (2001): 729-733.
12. Sane, Sanjay P. "The aerodynamics of insect flight." Journal of experimental biology 206.23 (2003): 4191-4208.
13. Hessler, Robert R. "Swimming in crustacea." Transactions of the Royal Society of Edinburgh: Earth Sciences 76.2-3 (1985): 115-122.
14. Kohlhage, K. "The economy of paddle-swimming: The role of added waters and viscosity in the locomotion of Daphnia magna." Zool. Beitr 35 (1994): 47-54.
15. Morris, M. J., K. Kohlhage, and G. Gust. "Mechanics and energetics of swimming in the small copepodAcanthocyclops robustus (Cyclopoida)."Marine Biology 107.1 (1990): 83-91.
16. Blaxter, John HS, et al. The biology of calanoid copepods. Vol. 33. Academic Press, 1998.
17. Knight-Jones, E. W., and A. Macfadyen. "The metachronism of limb and body movements in annelids and arthropods." Proc XVth Int Cong Zool(1959): 969-971.
18. Swadling, K. M., et al. "Respiration rate and cost of swimming for Antarctic krill, Euphausia superba, in large groups in the laboratory." Marine Biology146.6 (2005): 1169-1175.

19. Walker, Jeffrey A. "Functional morphology and virtual models: physical constraints on the design of oscillating wings, fins, legs, and feet at intermediate Reynolds numbers." Integrative and Comparative Biology 42.2 (2002): 232-242.
20. McHenry, Matthew J., and Jason Jed. "The ontogenetic scaling of hydrodynamics and swimming performance in jellyfish (Aurelia aurita)."Journal of Experimental Biology 206.22 (2003): 4125-4137.
21. Shorten, Marc, et al. "Kinematic analysis of swimming in Australian box jellyfish, Chiropsalmus sp. and Chironex fleckeri (Cubozoa, Cnidaria: Chirodropidae)." Journal of Zoology 267.4 (2005): 371-380.
22. Yu, Cheng-Lun, et al. "Three-dimensional numerical simulation of hydrodynamic interactions between pectoral-fin vortices and body undulation in a swimming fish." Physics of Fluids (1994-present) 23.9 (2011): 091901.
23. Hu, Huosheng, et al. "Design of 3D swim patterns for autonomous robotic fish." 2006 IEEE/RSJ International Conference on Intelligent Robots and Systems. IEEE, 2006.
24. Williams, Terri A. "A model of rowing propulsion and the ontogeny of locomotion in Artemia larvae." The Biological Bulletin 187.2 (1994): 164-173.
25. Sfakiotakis, Michael, and Dimitris P. Tsakiris. "Simuun: A simulation environment for undulatory locomotion." International Journal of Modelling and Simulation 26.4 (2006): 350-358.
26. Kils, Uwe. The swimming behavior, swimming performance and energy balance of Antarctic krill, Euphausia superba. No. 3. SCAR and SCOR, Scott Polar Research Institute, 1981.
27. Takagi, Daisuke. "Swimming with stiff legs at low Reynolds number."Physical Review E 92.2 (2015): 023020.

28. Gibb, Alice C., Kathryn A. Dickson, and George V. Lauder. "Tail kinematics of the chub mackerel Scomber japonicus: testing the homocercal tail model of fish propulsion." Journal of Experimental Biology 202.18 (1999): 2433-2447.
29. Nawroth, Janna C., et al. "A tissue-engineered jellyfish with biomimetic propulsion." Nature biotechnology 30.8 (2012): 792-797.
30. Murphy, David W., Donald R. Webster, and Jeannette Yen. "The hydrodynamics of hovering in Antarctic krill." Limnology and Oceanography: Fluids and Environments 3.1 (2013): 240-255.
31. Catton, Kimberly B., et al. "The hydrodynamic disturbances of two species of krill: implications for aggregation structure." Journal of Experimental Biology 214.11 (2011): 1845-1856.
32. Zhang, Calvin, et al. "Neural mechanism of optimal limb coordination in crustacean swimming." Proceedings of the National Academy of Sciences111.38 (2014): 13840-13845.
33. Hedrick, Tyson L. "Software techniques for two-and three-dimensional kinematic measurements of biological and biomimetic systems."Bioinspiration & biomimetics 3.3 (2008): 034001.
34. Murphy, D. W., et al. "Metachronal swimming in Antarctic krill: Gait kinematics and system design." Marine biology 158.11 (2011): 2541-2554.
35. Alben, Silas, et al. "Coordination of multiple appendages in drag-based swimming." Journal of The Royal Society Interface (2010): rsif20100171.
36. Lim, Jeanette L., and M. Edwin DeMont. "Kinematics, hydrodynamics and force production of pleopods suggest jet-assisted walking in the American lobster (Homarus americanus)." Journal of Experimental Biology 212.17 (2009): 2731-2745.
37. Clark, R. B., and D. J. Tritton. "Swimming mechanisms in nereidiform polychaetes." Journal of Zoology 161.2 (1970): 257-271.

APPENDICES

Schematic of physical model design

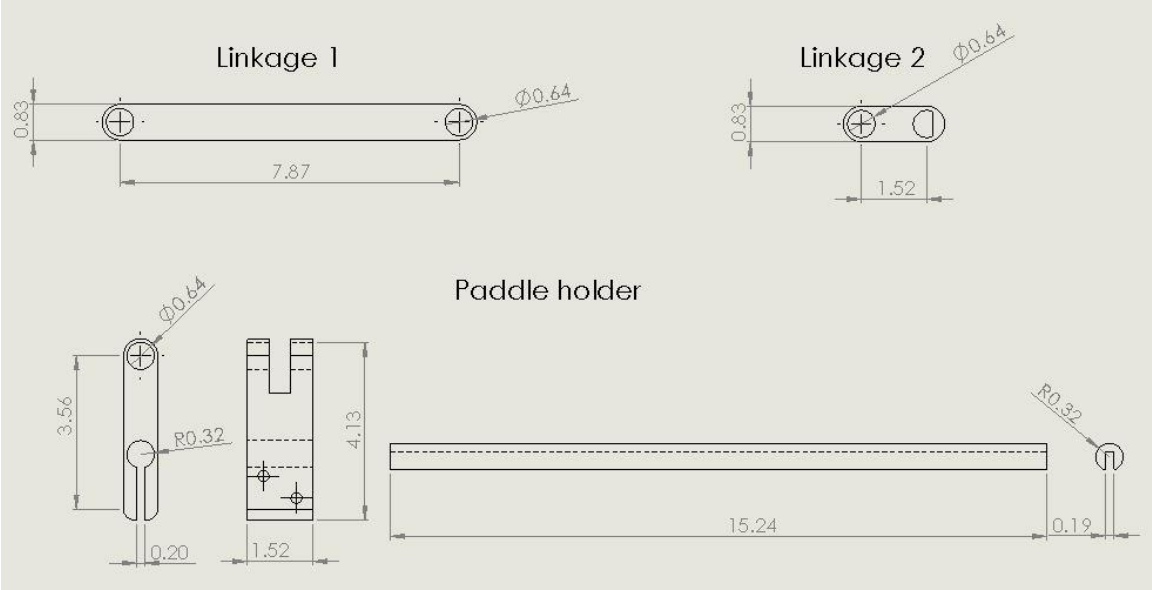

Showed few linkages and paddle holder used on four-bar mechanism on our physical model. All dimension shown above are in units of cm.

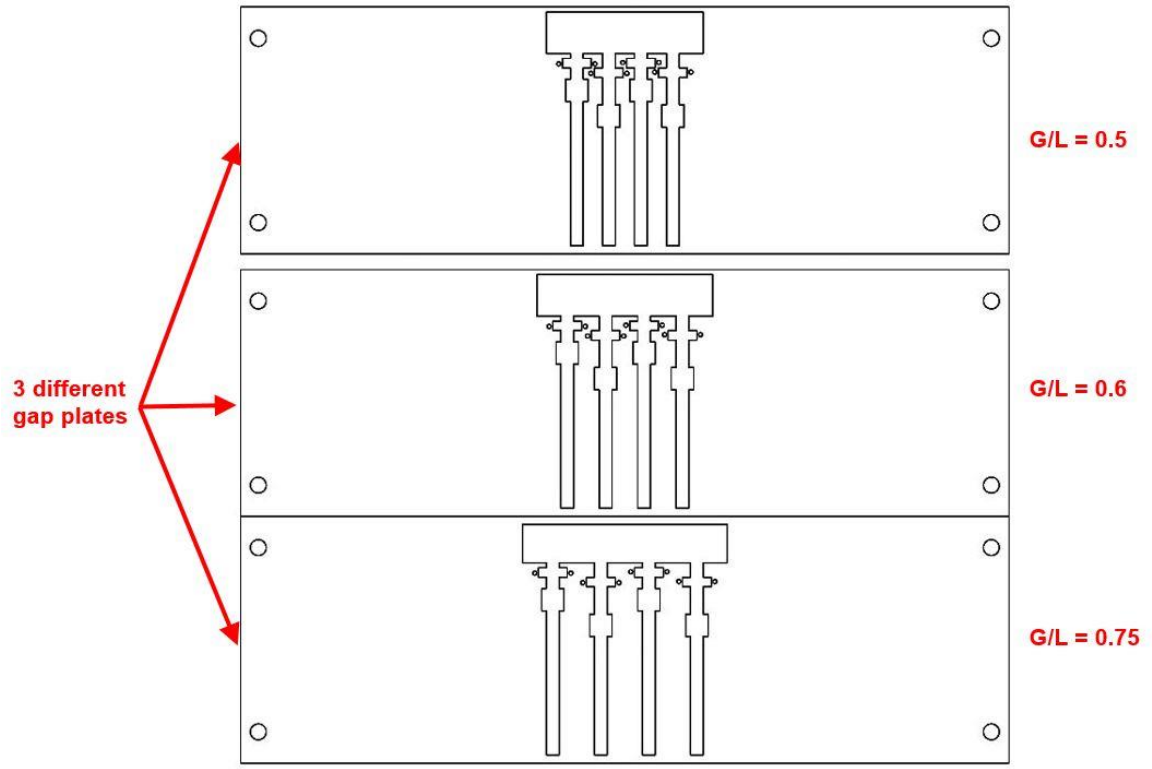

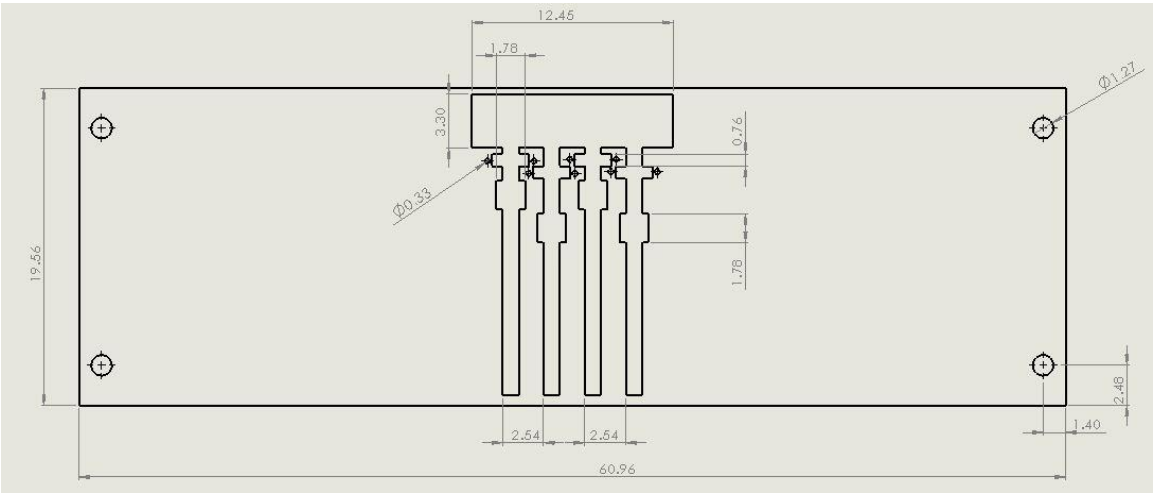

Three different gap plate design from our studies are shown above, and an example of gap plate schematic for G/L ratio of 0.5 are shown as well. All dimension shown above are in units of cm.

VITA

HONG KUAN LAI

Candidate for the Degree of

Master of Science

Thesis: PHYSICAL MODEL STUDIES OF METACHRONAL SWIMMING

Major Field: Mechanical Engineering

Biographical:

Education:

Completed the requirements for the Master of Science in Mechanical & Aerospace Engineering at Oklahoma State University, Stillwater, Oklahoma in December, 2016.

Completed the requirements for the Bachelor of Science in Mechanical Engineering at Oklahoma State University, Stillwater, Oklahoma in 2014.

Experience:

- Project leader at Applied Fluids Mechanics Lab (Stillwater, OK) from AUG2014 –present
- Designing bio-inspired system using SolidWorks/CAD for creating platform for future AUVs design.
- Experience in bio-system mechanical design, software control, statistical analysis and logical product development process.
- Writing, validation and verification protocols on new/existing processes based on experimental results.
- Maintaining proper and complete documentation which meets quality requirements.
- Working hands-on with junior engineers, technicians, collaborators and test systems.

Professional Memberships:

APS-DFD, Tau Sigma, Haliburton scholar